PAIN

Decreased abundance of TRESK two-pore domain potassium channels in sensory neurons underlies the pain associated with bone metastasis

Yue Yang[1,2]*, Song Li[1,2]*, Zi-Run Jin[1,2]*, Hong-Bo Jing[1,2]*, Hong-Yan Zhao[1,2], Bo-Heng Liu[1,2], Ya-Jing Liang[3], Ling-Yu Liu[1,2], Jie Cai[1,2], You Wan[1,2], Guo-Gang Xing[1,2,4†]

Cancer-associated pain is debilitating. Understanding the mechanisms that cause it can inform drug development that may improve quality of life in patients. Here, we found that the reduced abundance of potassium channels called TRESK in dorsal root ganglion (DRG) neurons sensitized nociceptive sensory neurons and cancer-associated pain. Overexpressing TRESK in DRG neurons suppressed tumor-induced neuronal hyperexcitability and pain hypersensitivity in bone metastasis model rats, whereas knocking down TRESK increased neuronal hyperexcitability and pain hypersensitivity in normal rats. Mechanistically, tumor-associated production of vascular endothelial growth factor (VEGF) activated the receptor VEGFR2 on DRGs, which increased the abundance of the calcineurin inhibitor DSCR1, which, in turn, decreased calcineurin-mediated activation of the transcription factor NFAT, thereby reducing the transcription of the gene encoding TRESK. Intrathecal application of exogenous calcineurin to tumor-bearing rats rescued TRESK abundance and abrogated both DRG hyperexcitability and pain hypersensitivity, whereas either inhibition or knockdown of calcineurin in normal rats reduced TRESK abundance and increased DRG excitability and pain sensitivity. These findings identify a potentially targetable mechanism that may cause bone metastasis–associated pain in cancer patients.

INTRODUCTION

Pain associated with cancer, particularly when tumors metastasize to bone, is often severe and debilitating (*1*). Mechanisms that underlie cancer-associated pain are elusive. Previously, we and others have reported that the sensitization of dorsal root ganglion (DRG) neurons contributes to the pathogenesis of bone metastasis–associated pain (*2*, *3*). TWIK-related spinal cord potassium channel (TRESK, also known as KCNK18 or K2P18.1) is a member of the two-pore domain potassium (K2P) channels, mediates major background currents in primary afferent neurons (*4*–*6*), and regulates neuronal excitability in both normal and disease states (*5*, *7*). Expression of mutant TRESK subunits increases (*8*), whereas overexpression of wild-type subunits reduces the excitability of trigeminal ganglion neurons (*9*). DRG neurons from TRESK functional knockout ("TRESK[ko]") mice exhibit decreased background K^+ currents and increased neuronal excitability relative to TRESK wild-type ("TRESK[wt]") mice (*5*). Spike frequency is attenuated in TRESK[wt] neurons but is augmented in TRESK[ko] neurons in response to the inflammation mediator lysophosphatidic acid (*10*). In animal models of neuropathic and inflammatory pain, TRESK abundance and TRESK-mediated background currents are decreased, and the excitability of DRG sensory neurons are enhanced (*7*, *11*). TRESK gene (*Kcnk18*) silencing by RNA interference increases animals' sensitivity to painful stimuli (*7*), whereas TRESK overexpression in DRG neurons attenuates nerve injury–induced mechanical allodynia in rats (*12*). These findings suggest that TRESK channels have a critical role in nociceptor excitability.

The TRESK channel is activated in response to cytoplasmic calcium signals by the calcium/calmodulin-dependent protein phosphatase called calcineurin (*13*–*15*). Calcineurin is anchored to a nuclear factor of activated T cells (NFAT)–like PQIIIS motif of human TRESK (PQIVID in the mouse protein) under resting conditions; in response to increased cytoplasmic calcium, it binds to the LQLP motif, which activates the channels by the dephosphorylation of the regulatory regions (*6*, *13*, *16*, *17*). Peripheral nerve injury may cause apparently antagonistic functions of calcineurin to work in concert (*18*, *19*) and then reduce the TRESK abundance (*20*). Loss of calcineurin in the spinal dorsal horn contributes to nerve injury–elicited neuropathic pain, which can be rescued by exogenous administration of calcineurin (*21*–*23*). Calcineurin is also a nociceptor modulator (*20*); activation of calcineurin reportedly might relieve pain by enhancing TRESK-mediated currents (*24*). In contrast, calcineurin inhibitors can induce severe pain hypersensitivity both in organ transplant patients (*25*–*28*) and in animal models (*29*, *30*), which is proposed to be at least partly due to an associated reduction in TRESK currents (*20*, *31*).

The endogenous calcineurin inhibitor DSCR1 (Down syndrome candidate region 1), also known as a regulator of calcineurin 1 (RCAN1), has been shown to be induced by vascular endothelial growth factor (VEGF) in a negative feedback loop to limit the calcineurin-NFAT signaling activity (*32*–*37*). In addition, VEGF–vascular endothelial growth factor receptor 2 (VEGFR2) signaling is also implicated in the pathogenesis of neuropathic pain (*38*). The proangiogenic factor VEGF-A_{165} sensitizes peripheral nociceptive neurons and increases the mechanical hypersensitivity to rats in a VEGFR2-dependent manner (*39*, *40*). VEGF also contributes to cancer-associated pain by activating VEGFR1 in sensory neurons (*41*). We hence hypothesized that the cancer-associated VEGF signaling–induced negative feedback inhibition of the calcineurin-NFAT signaling may subsequently

[1]Department of Neurobiology, School of Basic Medical Sciences and Neuroscience Research Institute, Peking University, Beijing 100083, China. [2]Key Laboratory for Neuroscience, Ministry of Education of China and National Committee of Health and Family Planning of China, Peking University, Beijing 100083, China. [3]Department of Oral and Maxillofacial Radiology, Peking University School and Hospital of Stomatology, Beijing 100081, China. [4]Second Affiliated Hospital of Xinxiang Medical University, Henan, China.
*These authors contributed equally to this work.
†Corresponding author. Email: ggxing@bjmu.edu.cn

decrease TRESK channel abundance in DRG neurons, thereby promoting cancer-associated pain. We explored this hypothesis using mammary rat metastasis tumor (MRMT-1) cells in a model of metastatic bone pain.

RESULTS

Decreased abundance of TRESK channels in DRG neurons is associated with increased pain sensitivity in bone metastasis model rats

To determine whether decreased TRESK channels in DRG neurons is responsible for the nociceptor sensitization and cancer pain development, we first examined the alterations of TRESK abundance, at the protein and messenger RNA (mRNA) levels, in ipsilateral L4/5 DRGs from rats 14 days after surgical implantation of rat breast carcinoma MRMT-1 cells into the tibial bone cavity (hereafter referred to as bone metastasis model rats or bone lesion–bearing rats). Using immunofluorescence staining and Western blotting, we found a substantial decrease in mean TRESK abundance in these neurons from tumor-bearing rats compared with controls (Fig. 1, A to C). Using real-time quantitative PCR (RT-qPCR), we saw a concomitant and substantial decrease in *TRESK* mRNA abundance (Fig. 1D). Moreover, despite no change in the frequency of TRESK expression among various types of DRGs, we calculated a significant reduction of TRESK immunofluorescence intensity in all types of neurons from MRMT-1–bearing rats relative to those from controls (fig. S1, A to C). The specificity of TRESK antibody was verified by using immunocytochemistry and Western blot, including a neutralizing peptide-blocking experiment with TRESK-transfected and nontransfected human embryonic kidney (HEK) 293 cells, which do not express endogenous TRESK (fig. S2).

Next, we examined the alterations of TRESK-mediated currents in nociceptive DRG neurons from bone metastasis model rats. TRESK currents were recorded on both $IB4^+$ and $IB4^-$, small DRG neurons, which were acutely dissociated from the ipsilateral L4/5 DRGs during days 14 to 18 after surgery. In $IB4^+$ DRG neurons, we observed a significant reduction of both the total background potassium currents (IK_{BG}) measured at +60 mV of a ramp voltage protocol and of the TRESK-containing standing outward potassium current (IK_{SO}) measured at −25 mV of a depolarizing step voltage protocol in tumor-bearing rats (Fig. 1, E and F). To further dissect currents through TRESK channels, we measured the percentage of outward currents that was sensitive to lamotrigine (a TRESK inhibitor) as described in previous studies (*42*). We found that the fraction of lamotrigine-sensitive currents was reduced in bone lesion–bearing rats at both the ramp voltage protocol and the depolarizing step voltage protocol (Fig. 1, G and H). Similarly, in $IB4^-$ DRG neurons, a significant decrease of TRESK currents was also observed in the ipsilateral L4/5 DRG neurons in the tumor-bearing rats (fig. S3, A and B). The fraction of lamotrigine-sensitive currents at both the voltage ramp and depolarizing step protocols was similarly declined in bone lesion–bearing rats (reduced by ~64 and ~45.7%, respectively; fig. S3, C and D).

Furthermore, we assessed spontaneous pain and its association with TRESK alteration in rats after tumor cell inoculation (Fig. 1, I to L). As expected, bone lesion–bearing rats exhibited robust behaviors associated with spontaneous pain, including a significant increase both in the number of flinches and in the time spent guarding on day 14 after surgery (Fig. 1, I and K). The correlation analysis between TRESK protein abundance and flinching ($r_{44} = -0.54$) or between TRESK protein abundance and guarding ($r_{45} = -0.48$) revealed that the TRESK abundance in the DRG was negatively correlated with spontaneous pain development in bone lesion–bearing rats (Fig. 1, J and L).

Overexpression of TRESK channels in DRG neurons reduces neuronal hyperexcitability and attenuates pain hypersensitivity in bone lesion–bearing rats

To further validate that the reduction of TRESK channels in DRG neurons underlies the pathogenesis of bone metastasis–associated pain, we examined the effects of TRESK overexpression on DRG neurons' excitability and pain sensitivity in bone lesion–bearing rats. Using immunofluorescence staining either of cultured DRG neurons after 48 hours of transfection with lentivirus expressing TRESK linked with ZsGreen (LV-TRESK) or of DRG tissues obtained from bone lesion–bearing rats on day 7 after intrathecal injection of LV-TRESK, we observed a prominent increase in the mean fluorescence intensity of TRESK immunostaining in LV-TRESK–infected DRG neurons in both the culture (~2.7-fold) and in situ (~2.1-fold) contexts compared with controls (fig. S4). Moreover, using Western blotting, we also found increased TRESK protein abundance in the LV-TRESK–infected DRGs (Fig. 2A). Meanwhile, the current density (in pA/pF) of both total background currents IK_{BG} and TRESK-containing IK_{SO} was increased in LV-TRESK–infected $IB4^+$ DRG neurons (Fig. 2, B and C) and $IB4^-$ DRG neurons (fig. S5, A to D).

In line with the functional augmentation of TRESK channels by LV-TRESK, we found a substantial decrease in bone lesion–induced neuronal hyperexcitability in LV-TRESK–infected DRG neurons. The increase in action potential (AP) numbers (spikes per second) in DRG neurons from bone lesion–bearing rats was significantly inhibited by intrathecal injection of LV-TRESK (Fig. 2, D and E, and fig. S5E). In addition, intrathecal delivery of LV-TRESK reversed the depolarized RMP and the reduced rheobase in the ipsilateral L4/5 DRG neurons of bone lesion–bearing rats (Fig. 2, F and G, and fig. S5, F and G).

The behavioral studies showed that overexpression of TRESK also alleviated the tumor-induced pain hypersensitivity in bone lesion–bearing rats. The decreased paw withdrawal threshold (PWT) to mechanical stimuli was significantly abrogated by intrathecal injection of LV-TRESK in MRMT-1 tumor-bearing rats 20 days after surgery (Fig. 2H). In contrast, intrathecal LV-TRESK in sham rats had no significant effect on animals' pain sensitivity (Fig. 2, H and I). Likewise, the increased spontaneous pain behaviors including flinching and guarding in tumor-bearing rats were significantly alleviated after intrathecal injection of LV-TRESK (Fig. 2, J and K). These results revealed that overexpression of TRESK in DRG neurons could effectively inhibit the tumor-induced neuronal hyperexcitability and pain hypersensitivity in bone lesion–bearing rats, suggesting that the reduction of TRESK channels in DRG neurons is involved in the pathogenesis of bone metastasis–associated pain.

Knockdown of TRESK channels in DRG neurons enhances the neuronal excitability and produces pain hypersensitivity in normal rats

Furthermore, we investigated whether knockdown of TRESK channels in DRG neurons using TRESK small interfering RNA (siRNA) could affect the neuronal excitability and pain sensitivity in normal rats. The specificity of TRESK siRNA was validated by RT-qPCR assay,

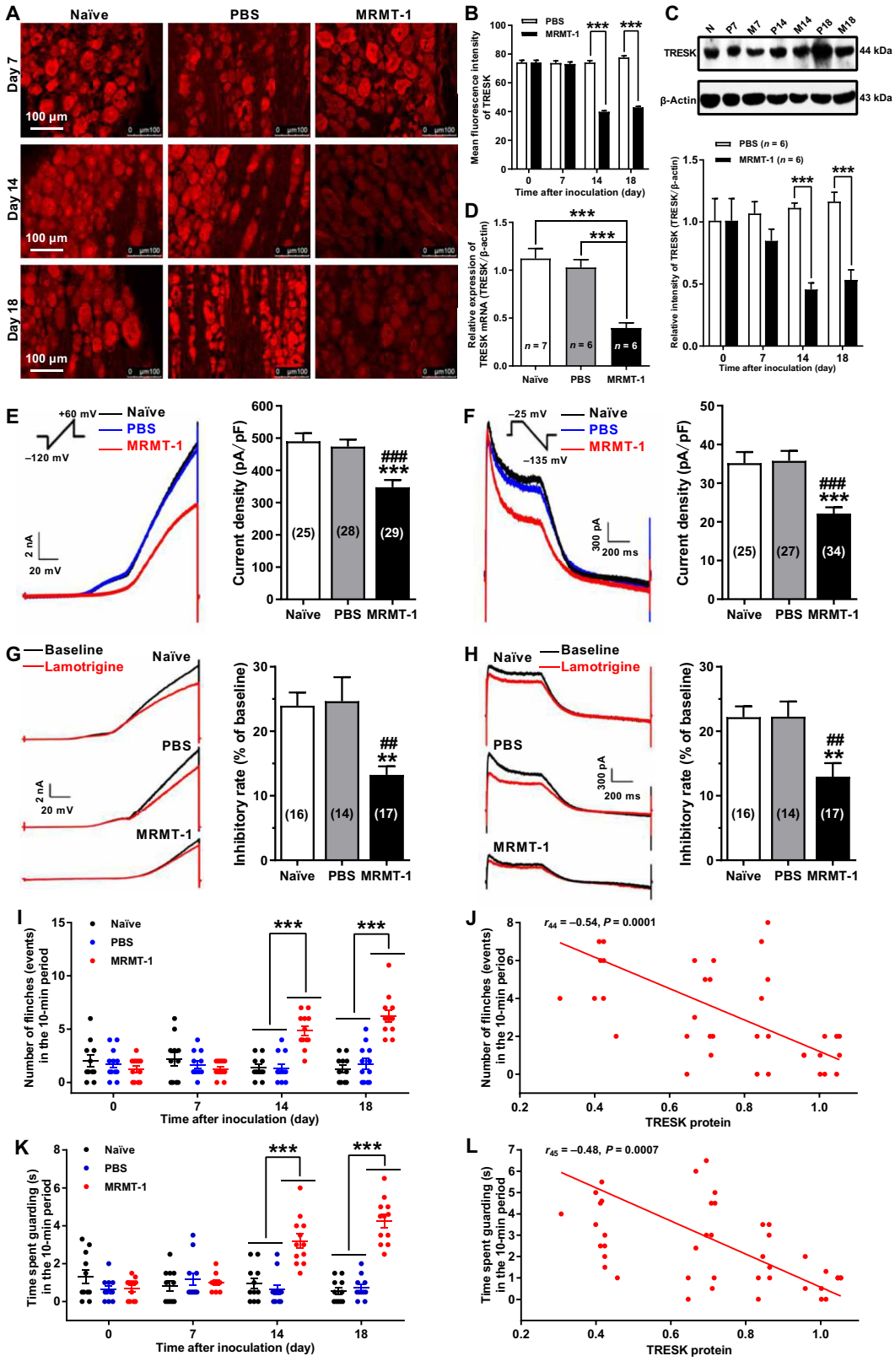

Fig. 1. Reduction of functional TRESK channels in DRG neurons and its association with pain in bone lesion–bearing rats. (**A** and **B**) TRESK immunofluorescence staining in ipsilateral L4/5 DRG neurons from naïve, phosphate-buffered saline (PBS)–injected, or bone-localized MRMT-1 tumor-bearing rats. Representative images (A) and a summary for the mean fluorescence intensity of TRESK immunostaining (B) are shown. n = 224 to 230 cells (from six rats) per time point per group. Two-way analysis of variance (ANOVA) followed by Bonferroni post hoc test: $F_{3,1818} = 116.2$, $^{***}P < 0.001$. (**C** and **D**) TRESK protein (C) and mRNA (D) abundance in the cells described in (A). n = 6 to 7 rats per time point per group. Two-way ANOVA followed by either Bonferroni post hoc test, $F_{3,40} = 4.21$ (C), or one-way ANOVA followed by Tukey post hoc test, $F_{2,16} = 20.54$ (D), $^{***}P < 0.001$. N, naïve; P, PBS; M, MRMT-1. (**E** and **F**) Representative TRESK current traces and a summary for the current density of both the total background currents (IK_{BG}) measured at +60 mV of a ramp voltage protocol (E) and the TRESK-containing IK_{SO} measured at −25 mV of a depolarizing step voltage protocol (F) in isolection B4–positive ($IB4^+$) ipsilateral L4/5 DRG neurons from naïve, PBS, or tumor-bearing rats. n = 25 to 34 cells (8 to 10 rats) per group. One-way ANOVA followed by Tukey post hoc test: $F_{2,79} = 11.61$ for IK_{BG} and $F_{2,83} = 12.18$ for IK_{SO}; $^{***}P < 0.001$, $^{\#\#\#}P < 0.001$ versus the corresponding naïve and PBS group, respectively. (**G** and **H**) The fraction of lamotrigine-sensitive currents in the cells described in (E) and (F). Representative current traces and a summary are shown. Currents were recorded in the presence of lamotrigine (100 μM) by the ramp voltage protocol (G) and the depolarizing step voltage protocol (H) as described in (E) and (F). n = 14 to 17 cells (from 8 to 10 rats) per group. One-way ANOVA followed by Tukey post hoc test: $F_{2,44} = 7.27$ for IK_{BG}; $F_{2,44} = 7.12$ for IK_{SO}; $^{**}P < 0.01$, $^{\#\#}P < 0.01$ versus the corresponding naïve and PBS group, respectively. (**I** to **L**) Correlation analysis between TRESK protein abundance and spontaneous pain behaviors in bone cancer rats. Spontaneous flinching (I) and guarding (K) behaviors were video recorded to assess the spontaneous pain in bone lesion–bearing rats (n = 11 to 12 rats per group). Two-way ANOVA followed by Bonferroni post hoc test: $F_{6,128} = 14.52$ for flinching; $F_{6,124} = 17.94$ for guarding; $^{***}P < 0.001$. (J) Correlation between flinching and TRESK protein abundance ($r_{44} = -0.54$, $P = 0.0001$). (L) Correlation between guarding and TRESK protein abundance ($r_{45} = -0.48$, $P = 0.0007$). The data of TRESK protein abundance in (J) and (L) are derived from the Western blot results shown (C).

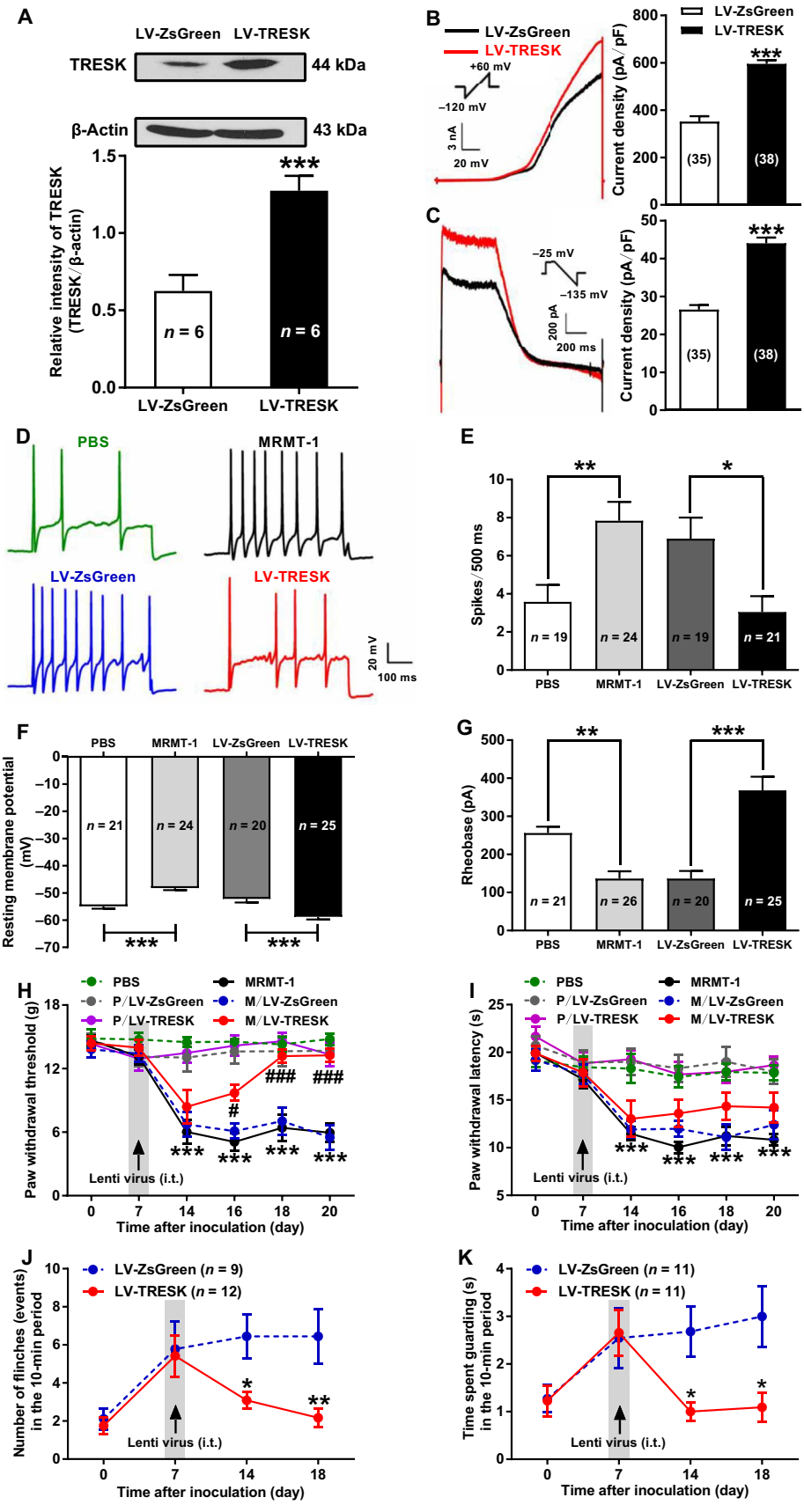

Fig. 2. Effects of TRESK overexpression on the tumor-induced reduction of functional TRESK channels, DRG neuron hyperexcitability, and pain hypersensitivity in bone cancer–bearing rats. (**A**) TRESK protein abundance in ipsilateral L4/5 DRGs of MRMT-1 tumor-bearing rats after intrathecally administered LV-TRESK. $n = 6$ rats per group. Two-tailed unpaired t test: $t_{10} = 4.57$, $^{***}P < 0.001$. (**B** and **C**) TRESK-containing currents in ipsilateral L4/5 DRG neurons in bone cancer–bearing rats after LV-TRESK application. Shown are representative current traces and a summary for the current density of both the total background currents (IK_{BG}) measured at +60 mV of a ramp voltage protocol (B) and the TRESK-containing IK_{SO} measured at −25 mV of a depolarizing step voltage protocol (C) in $IB4^+$ DRG neurons. $n = 35$ to 38 cells from 12 to 14 rats per group. Two-tailed unpaired t test: $t_{71} = 8.92$ for IK_{BG}, $t_{71} = 8.98$ for IK_{SO}, $^{***}P < 0.001$. (**D** to **G**) Effects of intrathecal (i.t.) LV-TRESK on the tumor-induced neuronal hyperexcitability in ipsilateral L4/5 DRG neurons of bone cancer–bearing rats. Representative traces of APs (D) and a summary for the spike number (E), the resting membrane potential (RMP) (F), and the rheobase for eliciting AP (G) in $IB4^+$ DRG neurons are shown. $n = 19$ to 26 cells from six to eight rats per group. One-way ANOVA followed by Tukey post hoc test: $F_{3,79} = 6.27$ for the AP numbers; $F_{3,86} = 20.97$ for the RMP; $F_{3,88} = 20.31$ for the rheobase; $^{*}P < 0.05$, $^{**}P < 0.01$, $^{***}P < 0.001$. (**H** and **I**) Effects of intrathecal LV-TRESK on the tumor-induced decrease in the PWT to mechanical stimuli (H) and the paw withdrawal latency (PWL) to thermal stimulation (I) in bone lesion–bearing rats. $n = 8$ to 12 rats per group. Two-way ANOVA followed by Bonferroni post hoc test: $F_{25,335} = 5.65$ for PWT; $F_{25,339} = 2.07$ for PWL; $^{***}P < 0.001$, $^{\#}P < 0.05$, $^{\#\#\#}P < 0.001$ versus the corresponding PBS and LV-ZsGreen group, respectively. (**J** and **K**) Effects of intrathecal LV-TRESK on the tumor-induced spontaneous pain in bone metastasis model rats. Flinching (J) and guarding (K) behaviors were video recorded to assess the spontaneous pain. $n = 9$ to 12 rats per group. Two-way ANOVA followed by Bonferroni post hoc test: $F_{3,76} = 2.43$ for flinching; $F_{3,80} = 2.75$ for guarding; $^{*}P < 0.05$, $^{**}P < 0.01$ versus the corresponding LV-ZsGreen group.

and the results demonstrated that, except for *TRESK* mRNA (decreased by ~73%; Fig. 3A), this siRNA could not reduce the abundance of mRNA encoding other K2P channels, including TWIK-related acid-sensitive potassium channel-1 (TASK1), TASK3, TWIK-related potassium channel 1 (TREK1), and TWIK-related arachidonic acid-activated potassium channel (TRAAK) (fig. S6), indicating that this siRNA selectively targeted *TRESK* mRNA. Western blotting analysis revealed that the TRESK protein abundance was significantly decreased (by ~53%) in the bilateral L4/5 DRGs in siRNA-treated rats (Fig. 3B), as were both the total background currents IK_{BG} and the TRESK-containing IK_{SO} in the $IB4^+$ DRG neurons (Fig. 3, C and D). In agreement with the functional reduction of TRESK channels in DRG neurons, we also observed a substantial increase in neuronal excitability, as indicated by increased AP numbers, a depolarized RMP, and reduced rheobase in rats treated with TRESK siRNA (Fig. 3, E to G). Likewise, intrathecal administration of TRESK siRNA also attenuated TRESK currents and enhanced excitability in $IB4^-$ DRG neurons from normal rats (fig. S7).

Behavioral analysis then showed that intrathecal administration of TRESK siRNA produced mechanical hypersensitivity, thermal hyperalgesia, and spontaneous pain in normal rats inferred from decreased PWT and PWL in the ipsilateral hindpaw in siRNA-treated rats relative to controls 2 days after siRNA injection (Fig. 3, H and I), and a significant increase in flinching and guarding of the ipsilateral hindpaw was also seen in TRESK siRNA-treated rats 1 day after siRNA injection (Fig. 3, J and K). These data indicate that knockdown of TRESK in DRG neurons reduces the TRESK-containing currents and subsequently induces neuronal hyperexcitability and pain hypersensitivity.

Decreased calcineurin abundance mediates the reduction of functional TRESK channels in DRG neurons from bone metastasis model rats

Activation of TRESK by calcineurin through dephosphorylation is a well-documented feature of TRESK channel regulation (*6*, *20*). Calcineurin has been shown to bind directly to the NFAT-like docking site on TRESK and activates the channel by the dephosphorylation of the two major regulatory regions at serine 264 and serine 276 "clusters" (*6*, *13*, *17*, *20*). Thus, the effect of TRESK dephosphorylation on NFAT-like docking sites can be inhibited by a calcineurin inhibitor such as cyclosporin A and tacrolimus (FK-506) (*20*). In agreement with this understanding, we found that exogenous application of either FK-506 (200 nM) or calcineurin siRNA (2 μg in a 10-μl volume) to DRG neurons for 24 hours could increase the phosphorylated TRESK abundance at the gross serine residues ($pTRESK^{ser}$) (no commercial antibody against phosphorylated TRESK at specific serine residue is available), both in cultured DRG neurons in vitro (1.43- ± 0.06-fold versus vehicle for FK-506; 1.46- ± 0.07-fold versus scramble for calcineurin siRNA) (fig. S8, A and B) and in the bilateral L4/5 DRGs of normal rats in vivo (1.55- ± 0.16-fold versus vehicle for FK-506; 1.39- ± 0.07-fold versus scramble for calcineurin siRNA) (fig. S8, C and D). In addition, we found that inhibition of TRESK dephosphorylation using the interfering peptide targeting serine 252, serine 262, serine 264, and serine 267 sites of TRESK, the identified dephosphorylation sites by calcineurin (*17*), could suppress the effects of calcineurin (10 enzyme units/μl × 10 μl) upon TRESK channels (fig. S9). For example, pretreatment of cultured DRG neurons with the interfering peptide TAT-Ser could significantly inhibit not only the calcineurin-induced increase both in TRESK protein abundance (decreased by 49.7 ± 8.2% versus the control peptide TAT-Ala) (fig. S9A) and in TRESK-containing currents (reduced by 21.9 ± 8.9% for IK_{BG} and by 32.8 ± 8.5% for IK_{SO} versus TAT-Ala) (fig. S9, B and C) but also the calcineurin-induced reduction of DRG neuron excitability (increased 2.32- ± 0.41-fold for the AP numbers, decreased by 8.3 ± 3.5% for the RMP, and reduced by 26.9 ± 9.6% for the rheobase versus TAT-Ala) (fig. S9, D to F). These results indicate that exogenous calcineurin may play its role through intracellular dephosphorylation of the TRESK channel in DRG neurons.

Furthermore, we found that, with FK-506 (200 nM), treatment to cultured DRG neurons also induced a significant decrease in both TRESK protein (decreased by 25.9 ± 3.7% at 48 hours) and mRNA (decreased by 45.5 ± 11.5% at 48 hours) abundance (versus vehicle; fig. S10, A and B). Together, these data suggested that calcineurin inhibition not only deactivates the TRESK channels through the suppression of TRESK dephosphorylation but also reduces the TRESK protein and mRNA abundance. In line with these findings, we observed that both the total background currents IK_{BG} [370.0 ± 19.9 pA/pF (FK-506) versus 452.6 ± 23.5 pA/pF (vehicle), $t_{52} = 2.69$, $P = 0.0097$] and the TRESK-containing IK_{SO} [34.8 ± 2.3 pA/pF (FK-506) versus 57.2 ± 5.1 pA/pF (vehicle)] were reduced in cultured DRG neurons with FK-506 treatment (fig. S10, C and D). In addition, an increased neuronal excitability was found in these FK-506-treated DRG neurons; e.g., the AP numbers were increased [2.1 ± 0.4 (FK-506) versus 1.0 ± 0.1 (vehicle)], the RMP was depolarized [−52.0 ± 0.9 mV (FK-506) versus −57.5 ± 0.5 mV (vehicle)], and the rheobase was decreased [64.9 ± 5.4 pA (FK-506) versus 90.2 ± 6.7 pA (vehicle)] in FK-506–treated DRG neurons (fig. S10, E to G). Moreover, an increased pain sensitivity as manifested by a reduced PWT [6.8 ± 3.4 g (FK-506) versus 13.5 ± 4.5 g (vehicle)] and PWL [18.8 ± 0.8 s (FK-506) versus 25.2 ± 1.1 s (vehicle)] was observed in rats that received intrathecal FK-506 treatment (on day 2 after drug injection; fig. S10, H and I). These results demonstrated that the calcineurin inhibition could reduce the functional TRESK abundance and enhance the neuronal excitability in cultured DRG neurons and produce pain hypersensitivity in normal rats.

Calcineurin is a calcium/calmodulin-dependent serine/threonine phosphatase that is activated by the elevation of intracellular calcium (*43*). Activated calcineurin triggers the dephosphorylation and the nuclear import of NFAT transcription factors and drives expression of multiple target genes (*44*). Hence, we supposed that the inhibition by FK-506 of calcineurin-mediated NFAT dephosphorylation is probably a potential mechanism underlying the reduction of TRESK protein and mRNA abundance upon application of the calcineurin inhibitor FK-506 (*45*). Because the dephosphorylation of NFAT is a prerequisite for its nuclear translocation, we thus examined the subcellular distribution of NFAT in cultured DRG neurons with FK-506 treatment (200 nM, for 24 hours). The results of Western blot analysis revealed that the amount of NFAT in the nuclear fraction was decreased (by 50.8 ± 3.4% versus vehicle) with FK-506 treatment (fig. S11A). The immunofluorescence staining using antibody specific to NFAT also showed that the nuclear localization of NFAT [the colocalization of NFAT and 4′,6-diamidino-2-phenylindole (DAPI)–stained nuclei] was significantly decreased with FK-506 incubation (fig. S11B). These data suggested that the activated calcineurin could promote TRESK abundance in an NFAT-dependent manner; thus, the calcineurin inhibition by FK-506 may reduce the TRESK protein and mRNA abundance, which is probably

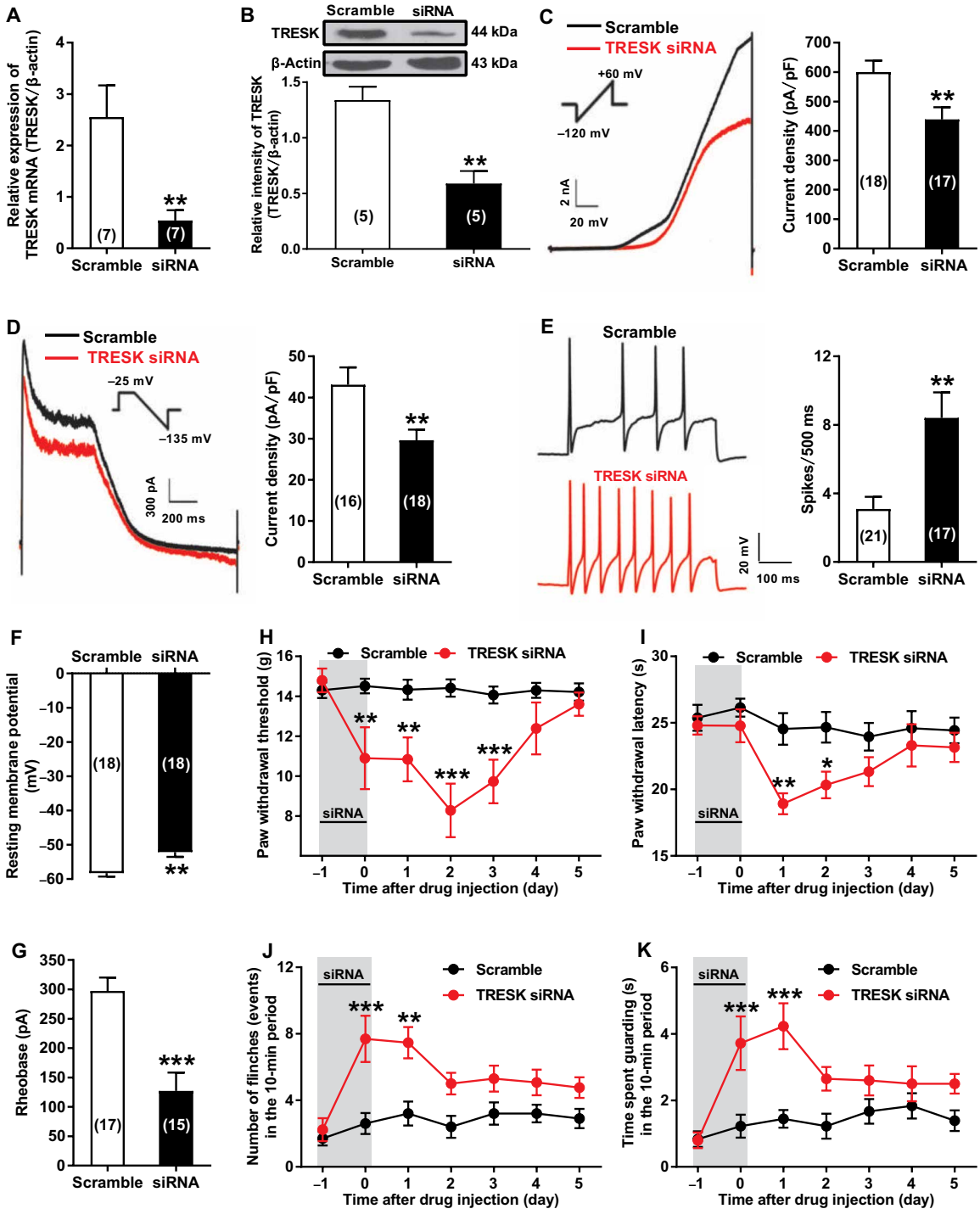

Fig. 3. Effects of TRESK knockdown on the abundance of functional TRESK channels, DRG neuron excitability, and pain sensitivity in normal rats. (**A** and **B**) TRESK abundance at the mRNA (A) and protein (B) levels in bilateral L4/5 DRGs after intrathecally administered TRESK siRNA. $n = 5$ to 7 rats per group. Two-tailed unpaired t test: $t_{12} = 3.12$ for TRESK mRNA, $t_8 = 4.55$ for TRESK protein, $^{**}P < 0.01$ versus the corresponding scramble group. (**C** and **D**) TRESK currents in bilateral L4/5 DRG neurons after TRESK siRNA application. Shown are representative current traces and a summary for the current density of both the total background currents (IK_{BG}) measured at +60 mV of a ramp voltage protocol (C) and the TRESK-containing IK_{SO} measured at −25 mV of a depolarizing step voltage protocol (D) in $IB4^+$ DRG neurons. $n = 16$ to 18 cells from six to seven rats per group. Two-tailed unpaired t test: $t_{33} = 2.84$ for IK_{BG}, $t_{32} = 2.81$ for IK_{SO}, $^{**}P < 0.01$. (**E** to **G**) Effects of intrathecal injection of TRESK siRNA on the neuronal excitability of bilateral L4/5 DRG neurons. Representative traces of APs and a summary for the spike number (E), the RMP (F), and the rheobase for eliciting AP (G) in $IB4^+$ DRG neurons are shown. $n = 15$ to 21 cells from six to seven rats per group. Two-tailed unpaired t test: $t_{36} = 3.43$ for the AP numbers; $t_{34} = 3.58$ for the RMP; $t_{30} = 4.49$ for the rheobase; $^{**}P < 0.01$, $^{***}P < 0.001$. (**H** and **I**) Effects of intrathecal TRESK siRNA on the PWT to mechanical stimuli (H) and the PWL to thermal stimulation (I) in normal rats. $n = 7$ to 11 rats per group. Two-way ANOVA followed by Bonferroni post hoc test: $F_{6,112} = 4.81$ for PWT; $F_{6,119} = 1.48$ for PWL; $^{*}P < 0.05$, $^{**}P < 0.01$, $^{***}P < 0.001$ versus the corresponding scramble group. (**J** and **K**) Effects of intrathecal TRESK siRNA on the spontaneous pain behaviors in normal rats. Flinching (J) and guarding (K) behaviors were video recorded to assess the spontaneous pain. $n = 9$ to 13 rats per group. Two-way ANOVA followed by Bonferroni post hoc test: $F_{6,147} = 1.88$ for flinching; $F_{6,119} = 2.51$ for guarding; $^{**}P < 0.01$, $^{***}P < 0.001$ versus the corresponding scramble group.

in part because of the disrupted NFAT dephosphorylation and nuclear translocation.

To further determine whether a decreased calcineurin mediates the reduction of TRESK channels and pain hypersensitivity caused by bone metastasis, we first examined the alteration of calcineurin abundance in DRGs from tumor-bearing rats. The results revealed that the abundance of calcineurin protein was notably decreased (by ~17% relative to controls) in the ipsilateral L4/5 DRGs on day

14 after surgery in bone-localized MRMT-1–bearing rats (Fig. 4A). Furthermore, we found that intrathecal administration of calcineurin rescued the tumor-induced reduction of both calcineurin and TRESK abundance in ipsilateral L4/5 DRG and abrogated the associated neuronal hyperexcitability and pain hypersensitivity. The abundance of both calcineurin and TRESK protein was modestly increased (Fig. 4, B and C), and *TRESK* mRNA expression was increased by just over twofold compared to the corresponding vehicle (Fig. 4D). The total background current IK_{BG} and the TRESK-containing IK_{SO} were both modestly augmented in calcineurin-treated rats compared with controls (Fig. 4, E and F). Furthermore, the AP number was decreased by ~67%, the RMP was hyperpolarized, and the rheobase increased by just over twofold on average in the calcineurin-treated rats (Fig. 4, G to I). Moreover, the ipsilateral PWT and PWL were significantly increased in calcineurin-treated rats (on day 17 after surgery; Fig. 4, J and K), implying that intrathecal calcineurin could attenuate the tumor-induced mechanical hypersensitivity and thermal hyperalgesia in bone lesion–bearing rats. In addition, we found that siRNA-mediated knockdown of TRESK prevented the exogenous calcineurin-induced augmentation of functional TRESK channels in the ipsilateral L4/5 DRG neurons of bone lesion–bearing rats (TRESK protein decreased by ~18%, IK_{BG} reduced by ~17%, and IK_{SO} reduced by ~23% relative to scramble-siRNA controls; fig. S12, A to D). Consistently, the decreased excitability of DRG neurons by exogenous calcineurin was also prevented in the tumor-bearing rats by pretreatment with TRESK siRNA (AP numbers increased ~2.6-fold, the RMP decreased by ~11%, and the rheobase reduced by ~42% relative to scramble-pretreated controls; fig. S12, E to G). Last, and likewise, the inhibitory effects of calcineurin on bone lesion–induced pain hypersensitivity were also disrupted by TRESK siRNA pretreatment: The PWT decreased from ~11.2 to ~5.8 g on average, and the PWL reduced from ~17.2 to 9.8 s on average relative to scramble-pretreated controls (fig. S12, H and I). These results indicate that exogenous calcineurin may suppress the development of bone metastasis–associated pain by enhancing the abundance of functional TRESK channels in DRG neurons.

On the other hand, we found that knockdown of calcineurin using intrathecal administration of calcineurin-targeted siRNA (fig. S13A) reduced the abundance of functional TRESK channels in DRG neurons and induced pain hypersensitivity in normal rats. The abundance of TRESK protein and mRNA was decreased in siRNA-treated rats compared with the scramble rats (fig. S13, B and C). Concordantly, the total background IK_{BG} and the TRESK-containing IK_{SO} currents were decreased (fig. S13, D and E), AP number was increased, RMP was depolarized, and the rheobase was decreased in siRNA-treated rats (fig. S13, F to H). Moreover, the ipsilateral PWT and PWL were significantly decreased in siRNA-treated rats (fig. S13, I and J). Collectively, these data suggest that a decreased calcineurin mediates the reduction of functional TRESK channels in DRGs of bone lesion–bearing rats, thereby contributing to the sensitization of nociceptive DRG neurons and tumor/bone metastasis–associated pain development.

To further test our hypothesis that the reduction of functional TRESK channels by a decreased calcineurin in DRG neurons in the bone metastasis model resulted from the disruption of the calcineurin-NFAT interaction, we performed additional experiments testing whether pretreatment with 11R-VIVIT (RRRRRRRRRRR-GG-MAGPHPVIVITGPHEE), an NFAT inhibitor peptide that selectively interferes with calcineurin-NFAT interaction without affecting the phosphatase activity of calcineurin (*46*, *47*), could effectively abrogate the inhibitory effects of exogenous calcineurin on the tumor-induced reduction of functional TRESK channels and induction of pain sensitivity in bone metastasis model rats. The calcineurin-induced augmentation of TRESK mRNA and protein abundance was decreased by ~63 and 20%, respectively, in VIVIT/calcineurin-treated bone lesion–bearing rats relative to the corresponding vehicle-treated group (Fig. 5, A and B). Likewise, the calcineurin-induced enhancement of both the total background current IK_{BG} and the TRESK-containing IK_{SO} was decreased by ~26 and 30%, respectively, in VIVIT/calcineurin-treated cancer rats relative to vehicle-treated rats (Fig. 5, C and D). DRGs from VIVIT/calcineurin-treated bone lesion–bearing rats also exhibited an increased AP number by about twofold, a depolarized RMP, and a decreased rheobase by ~44% (Fig. 5, E to G). In addition, the ipsilateral PWT and PWL were significantly decreased in VIVIT/calcineurin-treated cancer rats 1 day after VIVIT/calcineurin administration (Fig. 5, H and I).

In addition, we found that disrupting the calcineurin-NFAT interaction with VIVIT also reduced the abundance of functional TRESK channels in DRG neurons and induced pain hypersensitivity in normal rats. The abundance of TRESK mRNA and protein in the bilateral L4/5 DRGs from normal rats was markedly decreased (fig. S14, A and B), the total background IK_{BG} and TRESK-containing IK_{SO} currents were decreased (fig. S14, C and D), the AP number was increased (fig. S14E), the RMP was depolarized (fig. S14F), the rheobase was decreased (fig. S14G), and the ipsilateral PWT and PWL were significantly decreased (fig. S14, H and I) in VIVIT-treated rats relative to vehicle-treated rats. Together, these data suggested that the disruption of the calcineurin-NFAT interaction is a possible cause for the reduction of functional TRESK channels by a decreased calcineurin in DRG neurons from bone lesion–bearing rats.

VEGF contributes to calcineurin loss and subsequent reduction in functional TRESK channels and increase in DRG neuron excitability in culture

In endothelial cells, binding of VEGF to VEGFR2 enhances the abundance of the endogenous calcineurin inhibitor RCAN1 (also known as DSCR1), which triggers a negative feedback loop to inhibit the activity of calcineurin (*33*–*35*, *37*). VEGF also inhibits the augmentation of calcineurin and nuclear NFATc3 proteins in isoproterenol-treated neonatal rat ventricular cardiomyocytes (*48*). To test our hypothesis that the activation of VEGF-VEGFR2 signaling may induce calcineurin reduction and, hence, calcineurin loss–mediated TRESK reduction in DRG neurons from bone lesion–bearing rats, we first examined the effects of VEGF on calcineurin and TRESK protein abundance, on TRESK-containing currents, and on neuronal excitability in cultured DRG neurons. We found that exposure of cultured DRG neurons to VEGF (50 ng/ml) for 4 hours induced a significant decrease in the abundance of both calcineurin and TRESK protein (decreased by ~23 and ~35%, respectively, relative to vehicle-treated rats; fig. S15, A and B). These effects were inhibited either by co-application of VEGF-neutralizing antibody (VEGF-Ab; 1 μg/μl; fig. S15, A and B) or by pretreatment with calcineurin (10 enzyme units/μl; fig. S15C). Moreover, 11R-VIVIT (100 μM × 10 μl) also inhibited the VEGF-mediated reduction in TRESK protein abundance (about 1.7-fold) and mRNA (about 2-fold; fig. S15, D and E), suggesting that the VEGF-induced reduction in TRESK is likely dependent on the calcineurin–NFAT signaling pathway.

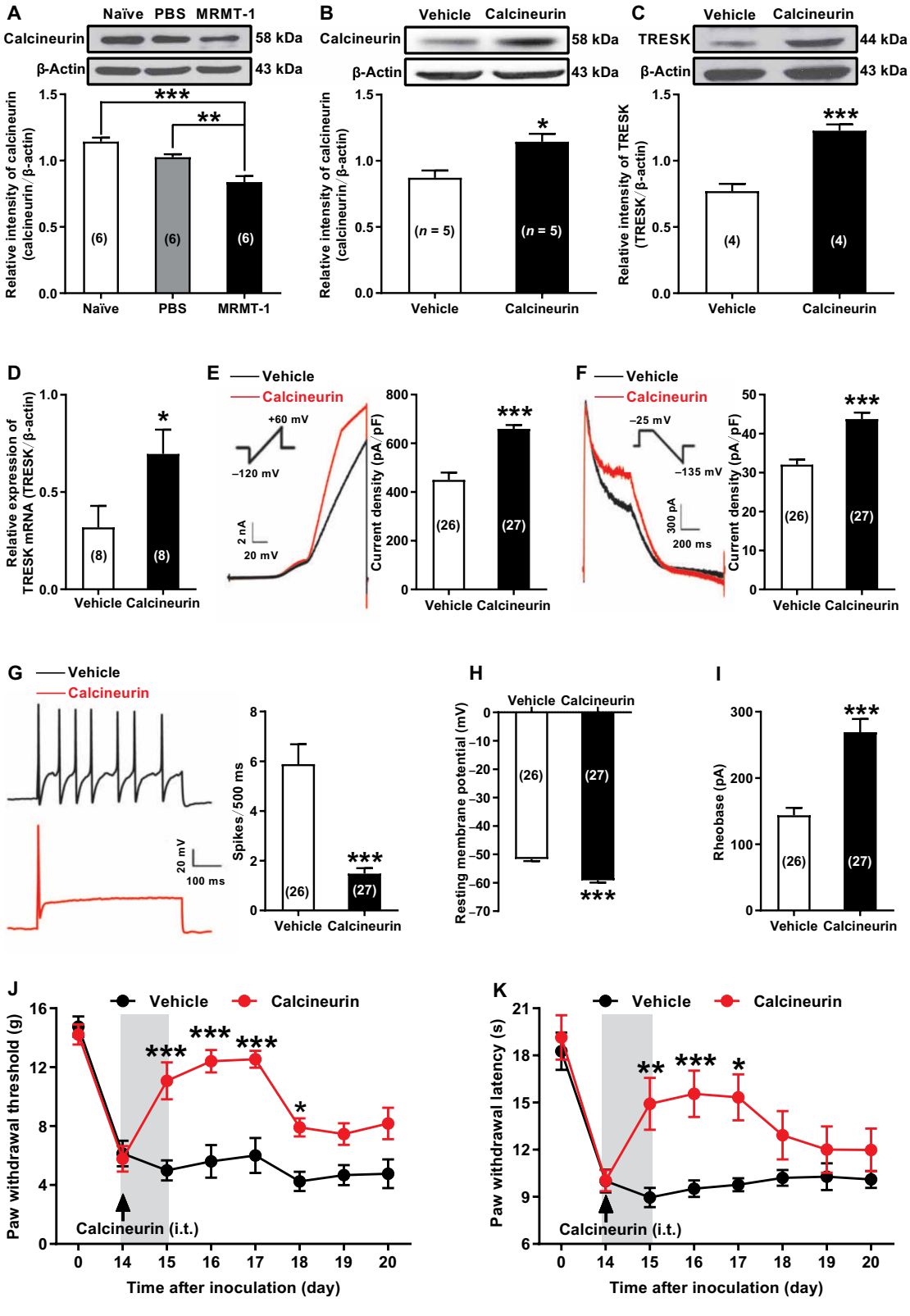

Fig. 4. Effects of intrathecal injection of calcineurin on the tumor-induced reduction of functional TRESK channels, DRG neuron hyperexcitability, and pain hypersensitivity in bone cancer–bearing rats. (**A**) Calcineurin protein abundance in ipsilateral L4/5 DRGs in naïve, PBS, and MRMT-1 tumor-bearing rats. $n = 6$ rats per group. One-way ANOVA followed by Tukey post hoc test: $F_{2,15} = 20.65$; $^{**}P < 0.01$, $^{***}P < 0.001$. (**B** to **D**) Effects of intrathecal injection of calcineurin on the tumor-induced decrease in the abundance of calcineurin (B), TRESK protein (C), and *TRESK* mRNA (D) in ipsilateral L4/5 DRGs of bone cancer rats. $n = 4$ to 8 biological replicates per group. Two-tailed unpaired t test: $t_8 = 3.36$ for calcineurin; $t_6 = 6.23$ and $t_{14} = 2.26$ for TRESK protein and mRNA, respectively; $^{*}P < 0.05$, $^{***}P < 0.001$. (**E** and **F**) Effects of intrathecal calcineurin on the tumor-induced reduction of TRESK-containing currents in ipsilateral L4/5 DRG neurons of bone cancer–bearing rats. Shown are representative current traces and a summary for the current density of both the total background currents (IK_{BG}) measured at +60 mV of a ramp voltage protocol (E) and the TRESK-containing IK_{SO} measured at −25 mV of a depolarizing step voltage protocol (F) in $IB4^+$ DRG neurons. $n = 26$ to 27 cells from eight to nine rats per group. Two-tailed unpaired t test: $t_{51} = 6.24$ for IK_{BG}, $t_{51} = 5.51$ for IK_{SO}; $^{***}P < 0.001$. (**G** to **I**) Effects of intrathecal calcineurin on the tumor-induced neuronal hyperexcitability in ipsilateral L4/5 DRG neurons of bone cancer–bearing rats. Representative traces of APs and a summary for the spike number (G), the RMP (H), and the rheobase for eliciting AP (I) in $IB4^+$ DRG neurons are shown. $n = 26$ to 27 cells from eight to nine rats per group. Two-tailed unpaired t test: $t_{51} = 5.38$ for the AP numbers; $t_{51} = 6.66$ for the RMP; $t_{51} = 5.46$ for the rheobase; $^{***}P < 0.001$. (**J** and **K**) Effects of intrathecal calcineurin on the tumor-induced decrease in the PWT to mechanical stimuli (J) and the PWL to thermal stimulation (K) in bone cancer rats. $n = 13$ to 14 rats per group. Two-way ANOVA followed by Bonferroni post hoc test: $F_{7,160} = 6.20$ for PWT; $F_{7,140} = 2.29$ for PWL; $^{*}P < 0.05$, $^{**}P < 0.01$, $^{***}P < 0.001$ versus the corresponding vehicle group.

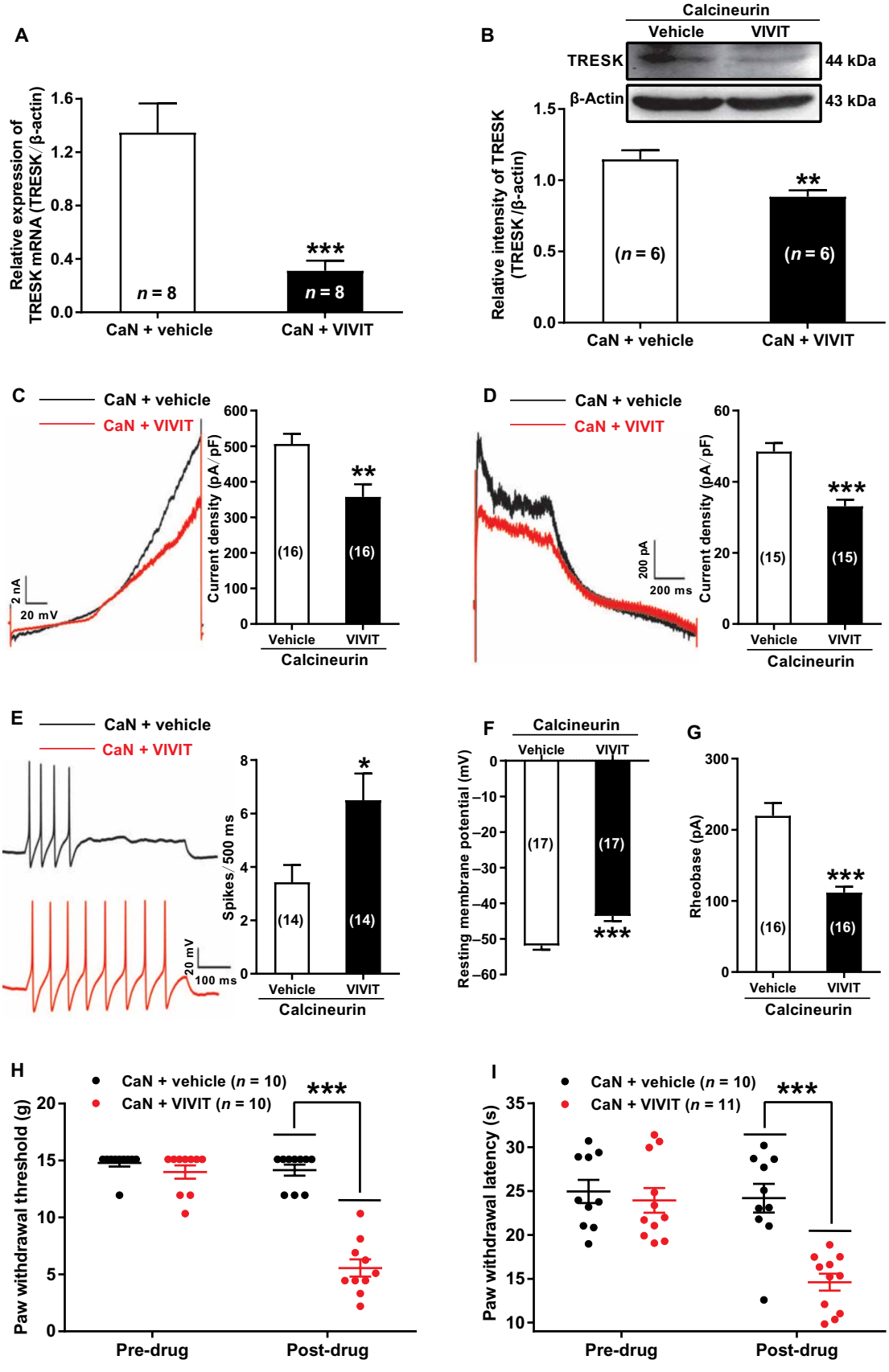

Fig. 5. Effects of pretreatment with NFAT inhibitor peptide on the calcineurin-induced alterations of TRESK abundance, DRG excitability, and pain sensitivity in bone cancer–bearing rats. (**A** and **B**) Effects of pretreatment with the NFAT inhibitor peptide VIVIT on the calcineurin (CaN)–induced increase in *TRESK* mRNA (A) and TRESK protein (B) abundance in ipsilateral L4/5 DRGs of bone cancer–bearing rats. $n = 6$ to 8 rats per group. Two-tailed unpaired t test: $t_{14} = 4.49$ for *TRESK* mRNA; $t_{10} = 3.32$ for TRESK protein; $^{**}P < 0.01$, $^{***}P < 0.001$. (**C** and **D**) Effects of pretreatment with VIVIT on the calcineurin-induced augmentation of TRESK-containing currents in ipsilateral L4/5 DRG neurons of bone cancer–bearing rats. Shown are representative current traces and a summary for the current density of both the total background currents (IK_{BG}) measured at +60 mV of a ramp voltage protocol (C) and the TRESK-containing IK_{SO} measured at −25 mV of a depolarizing step voltage protocol (D) in $IB4^+$ DRG neurons. $n = 15$ to 16 cells from four to five rats per group. Two-tailed unpaired t test: $t_{30} = 3.26$ for IK_{BG}; $t_{28} = 5.08$ for IK_{SO}; $^{**}P < 0.01$, $^{***}P < 0.001$. (**E** to **G**) Effects of pretreatment with VIVIT on the calcineurin-induced reduction of DRG neuron excitability in ipsilateral L4/5 DRG neurons in tumor-bearing rats. Representative traces of APs and a summary for the spike number (E), the RMP (F), and the rheobase for eliciting AP (G) in $IB4^+$ DRG neurons are shown. Two-tailed unpaired t test: $t_{26} = 2.59$ for the AP numbers; $t_{32} = 4.38$ for the RMP; $t_{30} = 5.46$ for the rheobase; $^{*}P < 0.05$, $^{***}P < 0.001$. (**H** and **I**) Effects of pretreatment with VIVIT on the calcineurin-induced increase in the PWT to mechanical stimuli (H) and the PWL to thermal stimulation (I) in bone cancer–bearing rats. $n = 10$ to 11 rats per group. Two-way ANOVA followed by Bonferroni post hoc test: $F_{1,36} = 48.97$ for PWT, $F_{1,38} = 10.12$ for PWL, $^{***}P < 0.001$.

Consistently, VEGF also induced a significant decrease in both the total background currents IK_{BG} and the TRESK-containing IK_{SO} (decreased by ~28 and ~37%, respectively) relative to vehicle-treated rats. These effects were reversed by pretreatment with calcineurin or VEGF-Ab (fig. S15, F and G). In addition, VEGF induced a significant increase in DRG neuron excitability (relative to vehicle, the AP numbers increased ~2-fold, the change in RMP indicated depolarization by ~6%, and the rheobase decreased by ~29%) but was abrogated by pretreatment with calcineurin or VEGF-Ab (fig. S15, H to K). These results suggest that VEGF may suppress the abundance of functional TRESK channels and, consequently, increase excitability in DRG neurons through the reduction of calcineurin.

Inhibition of VEGF signaling reverses the tumor-induced reduction of calcineurin and TRESK abundance in DRG neurons and alleviates pain hypersensitivity in bone lesion–bearing rats

To further investigate whether signaling by VEGF through VEGFR2 is critical for the calcineurin-mediated TRESK reduction in DRG neurons and the consequent pain hypersensitivity induced by bone metastasis, we first examined the alterations of VEGF and VEGFR2 protein abundance in tumor-bearing rats. The results revealed that the abundance of both VEGF and VEGFR2 protein in the ipsilateral L4/5 DRGs was significantly increased 2 weeks after bone lesion implantation (Fig. 6, A and B). In agreement with these findings, we found that exogenous VEGF reduced the abundance of calcineurin and TRESK proteins, enhanced DRG neuron excitability, and increased pain sensitivity in normal rats. The abundance of calcineurin and TRESK proteins was decreased (by ~13 and ~24%, respectively) in VEGF-treated rats compared with vehicle-treated rats (Fig. 6, C and D). In addition, the total background current IK_{BG} and the TRESK-containing IK_{SO} were decreased by ~28 and ~49%, respectively, in VEGF-treated rats (Fig. 6, E and F), the AP numbers (spikes per second) were increased, the RMP exhibited a depolarized shift, and the rheobase was decreased (by ~55%) in VEGF-treated rats (Fig. 6, G to I). In addition, the ipsilateral PWT and PWL were significantly decreased in VEGF-treated rats 2 days after VEGF treatment (Fig. 6, J and K).

Following on from those results, we assessed the effects of a VEGF-Ab and a VEGFR2 inhibitor (Ki8751) on the abundance of calcineurin and TRESK, the TRESK-containing currents and hyperexcitability in DRG neurons, and the pain hypersensitivity in bone lesion–bearing rats. We found that intrathecal administration of either VEGF-Ab (fig. S16) or Ki8751 (Fig. 7) modestly reversed the tumor-induced reduction of both calcineurin and TRESK protein abundance in the ipsilateral L4/5 DRGs (~1.4-fold and ~1.6- to 1.8-fold, respectively; fig. S16, A and B, and Fig. 7, A and B). Consistently, the tumor-induced decrease in both the background current IK_{BG} and the TRESK-containing IK_{SO} was also rescued by either VEGF-Ab or Ki8751 (fig. S16, C and D, and Fig. 7, C and D). In addition, VEGF-Ab or Ki8751 rescued the AP number, RMP, and rheobase in ipsilateral L4/5 DRG neurons from bone lesion–bearing rats (fig. S16, E to G, and Fig. 7, E to G). Moreover, both VEGF-Ab and Ki8751 abrogated the tumor-induced pain hypersensitivity in bone lesion–bearing rats, as inferred from an increased PWT in response to mechanical stimuli and PWL in response to thermal stimulation (fig. S16, H and I, and Fig. 7, H and I). These results indicate that the activation of VEGF-VEGFR2 signaling induces the decrease in calcineurin that consequently reduces the abundance of functional TRESK channels in DRG neurons, which promotes the development of pain hypersensitivity in bone lesion–bearing rats.

DISCUSSION

We here provide multiple lines of evidence to show that decreased TRESK channels in DRG neurons contribute to the cancer pain development. First, we found a reduction of functional TRESK channels in DRG neurons and its association with pain hypersensitivity in bone lesion–bearing rats. Second, we discovered that TRESK overexpression rescued the tumor-induced hyperexcitability of DRG neurons and pain hypersensitivity in bone lesion–bearing rats, whereas TRESK knockdown enhanced the neuronal excitability and produced pain hypersensitivity in normal rats. These findings are consistent with previous reports that TRESK channels play a critical role in determining neuronal excitability of primary sensory neurons (*5*, *10*); therefore, a decreased TRESK would result in the DRG neurons' hyperexcitability and pain hypersensitivity under pathologic conditions (*7*, *10*, *11*). TRESK is one of the major background potassium channels that contribute to DRG neurons' RMP (*5*). Similar to our previous findings (*3*), alterations of intrinsic membrane properties including a depolarized RMP shift and a decreased rheobase for eliciting AP, which are associated with enhanced neuronal excitability, were observed in cancer rat DRG neurons, and importantly, all these alterations were reversed by overexpressing TRESK in tumor-bearing rats. Conversely, knockdown of TRESK in normal rats could induce a depolarized RMP and a decreased rheobase as evident in tumor-bearing animals. These results indicated that TRESK reduction may result in a depolarized RMP shift and a decreased rheobase, thereby contributing to DRG neuron hyperexcitability and pain hypersensitivity in bone lesion–bearing rats.

Activation of TRESK by calcineurin through dephosphorylation is a well-documented feature of TRESK channel regulation (*6*, *20*). Calcineurin can bind directly to the NFAT-like docking site on TRESK and activate it by the dephosphorylation of the channel (*6*, *13*, *17*, *20*). We found that both calcineurin inhibitor (FK-506) and siRNA could inhibit the dephosphorylation of TRESK in DRG neurons and that inhibition of TRESK dephosphorylation by an interfering peptide could disrupt the modulation of calcineurin on TRESK channels. Moreover, we found that FK-506 treatment for cultured DRG neurons also induced a reduction of TRESK protein and mRNA abundance. These data suggested that calcineurin inhibition not only deactivated the TRESK channel through suppressing TRESK dephosphorylation but also decreased the TRESK abundance. Calcineurin is a calcium/calmodulin-dependent serine/threonine phosphatase that is activated by an increase in intracellular calcium (*43*). Activated calcineurin triggers the dephosphorylation and the nuclear import of NFAT transcription factors and drives expression of multiple target genes (*44*). We thus suggested that the inhibition of calcineurin-mediated NFAT dephosphorylation by FK-506 is a potential mechanism underlying the reduction of TRESK protein and mRNA abundance upon FK-506 application (*45*). In support of our understanding, we indeed found that, as an inevitable result of NFAT dephosphorylation, the nuclear translocation of NFAT was reduced with FK-506 treatment for cultured DRG neurons.

In addition, we provide further evidence demonstrating that a decreased calcineurin mediates TRESK reduction in cancer rat DRG neurons. We found that repression of calcineurin with FK-506

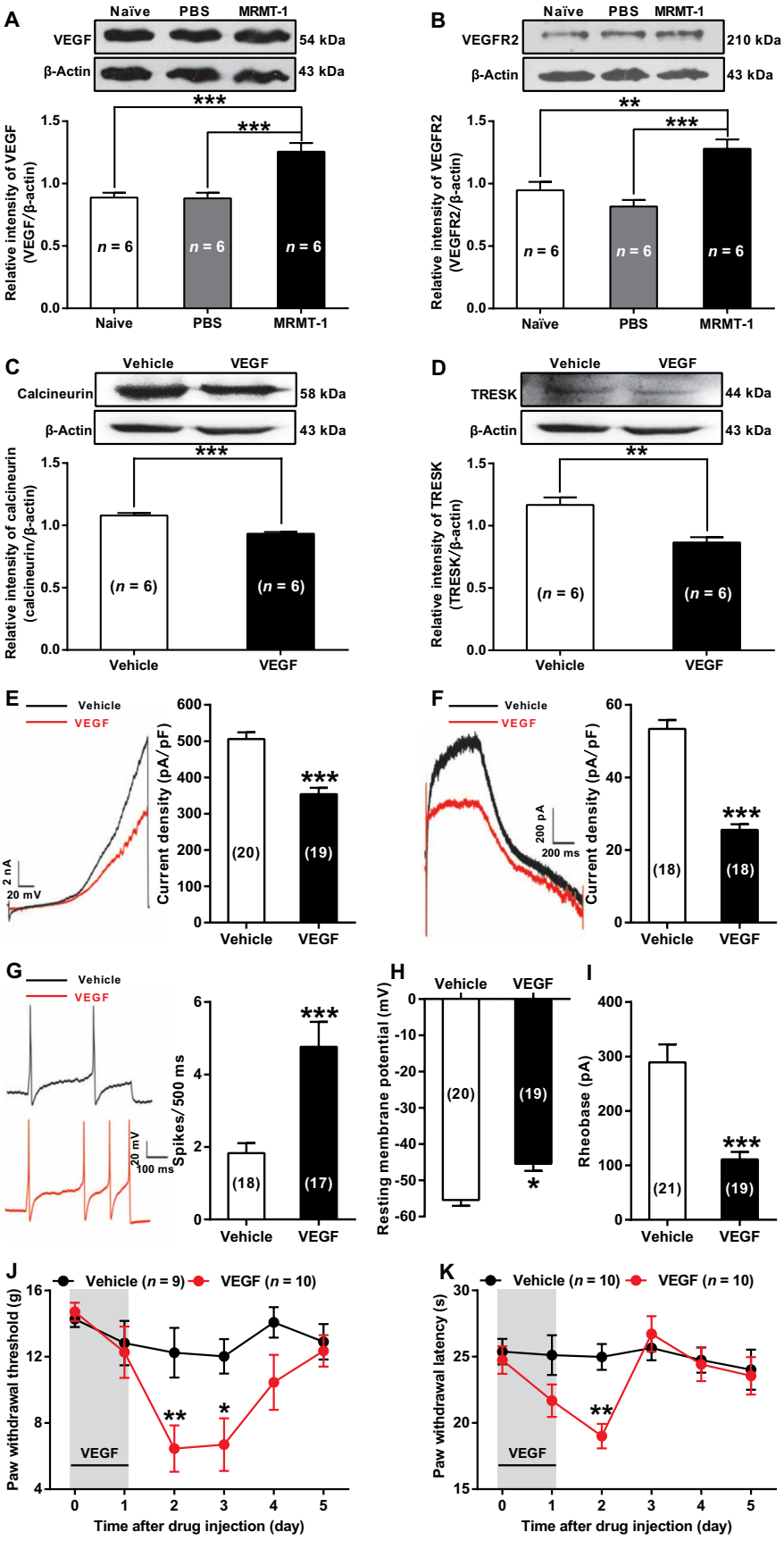

Fig. 6. The abundance of VEGF and VEGFR2 in ipsilateral L4/5 DRGs in bone cancer–bearing rats, and the effect of intrathecal injection of VEGF on the functional TRESK abundance, DRG neuron excitability, and pain sensitivity in normal rats. (**A** and **B**) VEGF and VEGFR2 protein abundance in ipsilateral L4/5 DRGs in naïve, PBS, and MRMT-1 tumor-bearing rats. $n = 6$ rats per group. One-way ANOVA followed by Tukey post hoc test: $F_{2,15} = 16.45$ for VEGF; $F_{2,15} = 13.27$ for VEGFR2; $^{**}P < 0.01$, $^{***}P < 0.001$. (**C** and **D**) Effects of intrathecal injection of VEGF on calcineurin and TRESK abundance in bilateral L4/5 DRGs of normal rats. $n = 6$ rats per group. Immunoblots shown are from the same membrane, reblotted for TRESK. Two-tailed unpaired t test: $t_{10} = 5.90$ for calcineurin; $t_{10} = 4.05$ for TRESK; $^{**}P < 0.01$, $^{***}P < 0.001$. (**E** and **F**) Effects of intrathecal VEGF on TRESK-containing currents in bilateral L4/5 DRG neurons of normal rats. Shown are representative current traces and a summary for the current density of both the total background currents (IK_{BG}) measured at +60 mV of a ramp voltage protocol (E) and the TRESK-containing IK_{SO} measured at −25 mV of a depolarizing step voltage protocol (F) in $IB4^+$ DRG neurons. $n = 18$ to 20 cells from five to six rats per group. Two-tailed unpaired t test: $t_{37} = 5.92$ for IK_{BG}, $t_{34} = 9.68$ for IK_{SO}, $^{***}P < 0.001$. (**G** to **I**) Effects of intrathecal VEGF on the neuronal excitability of bilateral L4/5 DRG neurons in normal rats. Representative traces of APs and a summary for the spike number (G), the RMP (H), and the rheobase for eliciting AP (I) in $IB4^+$ DRG neurons are shown. $n = 17$ to 21 cells from five to six rats per group. Two-tailed unpaired t test: $t_{33} = 4.04$ for the APs; $t_{37} = 4.00$ for the RMP; $t_{38} = 4.82$ for the rheobase; $^{*}P < 0.05$, $^{***}P < 0.001$. (**J** and **K**) Effects of intrathecal VEGF on the PWT to mechanical stimuli (J) and the PWL to thermal stimulation (K) in normal rats. $n = 9$ to 10 rats per group. Two-way ANOVA followed by Bonferroni post hoc test: $F_{5,102} = 2.32$ for PWT; $F_{5,108} = 2.35$ for PWL; $^{*}P < 0.05$, $^{**}P < 0.01$.

indeed resulted in a reduction of functional TRESK channels and an enhanced neuronal excitability in cultured DRG neurons and that intrathecal FK-506 produced pain hypersensitivity in normal rats. These results presented a convincing explanation for the underlying mechanisms of CIPS, a calcineurin inhibitor–induced pain syndrome (*29*), by which the calcineurin inhibitor may exert its action via TRESK suppression in DRG neurons. Actually, we found a significant reduction of calcineurin abundance in DRGs from bone lesion–bearing rats and that intrathecal delivery of exogenous calcineurin could reverse the tumor-induced TRESK reduction in DRG neurons and subsequently abrogated neuronal hyperexcitability and pain hypersensitivity. Similarly, Miletic *et al.* (*21*) have reported that intrathecal administration of calcineurin alleviates pain hypersensitivity in neuropathic rats. In support of the notion that the TRESK channel is a downstream transcriptional target of calcineurin signaling (*13*), we provided additional evidence showing that intrathecal delivery of TRESK siRNA could inhibit the calcineurin's action in bone lesion–bearing rats.

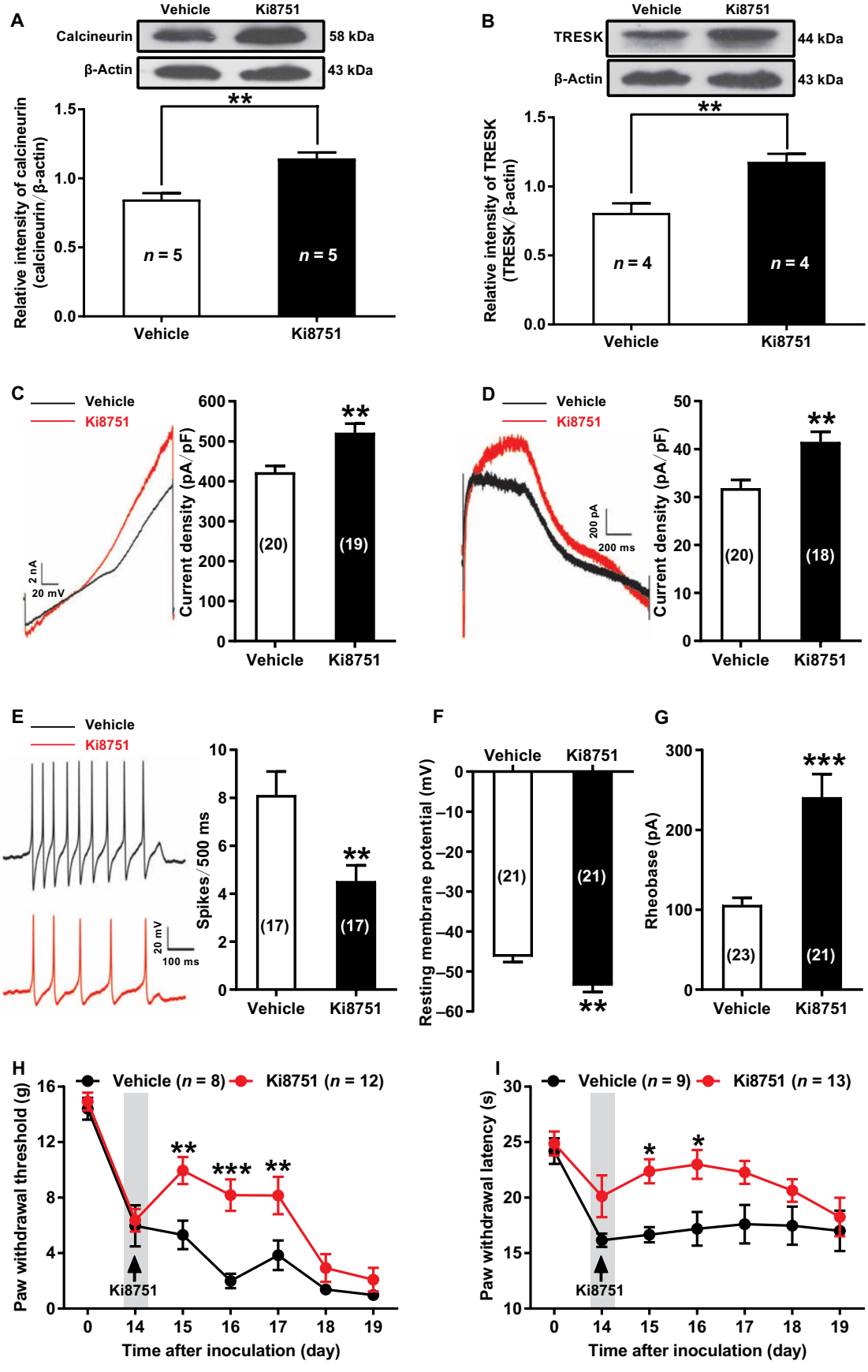

Fig. 7. Effects of VEGFR2 inhibitor on the abundance of calcineurin and TRESK, DRG neuron excitability, and pain hypersensitivity in rats with bone cancer. (**A** and **B**) Effects of intrathecal injection of Ki8751 on the tumor-induced reduction of calcineurin and TRESK protein abundance in ipsilateral L4/5 DRGs of bone cancer–bearing rats. $n = 4$ to 5 rats per group. Two-tailed unpaired t test: $t_8 = 4.58$ for calcineurin, $t_{12} = 4.06$ for TRESK, $^{**}P < 0.01$. (**C** and **D**) Effects of intrathecal Ki8751 on the tumor-induced decrease in TRESK-containing currents in ipsilateral L4/5 DRG neurons of bone cancer–bearing rats. Shown are representative current traces and a summary for the current density of both the total background currents (IK_{BG}) measured at +60 mV of a ramp voltage protocol (C) and the TRESK-containing IK_{SO} measured at −25 mV of a depolarizing step voltage protocol (D) in $IB4^+$ DRG neurons. $n = 18$ to 20 cells from five to six rats per group. Two-tailed unpaired t test: $t_{37} = 3.59$ for IK_{BG}, $t_{36} = 3.54$ for IK_{SO}, $^{**}P < 0.01$. (**E** to **G**) Effects of intrathecal Ki8751 on the tumor-induced enhancement of DRG neuron excitability in bone cancer–bearing rats. Representative traces of APs and a summary for the spike number (E), the RMP (F), and the rheobase for eliciting AP (G) in $IB4^+$ DRG neurons are shown. $n = 17$ to 23 cells from five to six rats per group. Two-tailed unpaired t test: $t_{32} = 3.04$ for the AP numbers; $t_{40} = 3.49$ for the RMP; $t_{42} = 4.60$ for the rheobase; $^{**}P < 0.01$, $^{***}P < 0.001$. (**H** and **I**) Effects of intrathecal Ki8751 on the tumor-induced decrease in the PWT to mechanical stimuli (H) and the PWL to thermal stimulation (I) in bone cancer–bearing rats. $n = 8$ to 13 rats per group. Two-way ANOVA followed by Bonferroni post hoc test: $F_{6,131} = 2.85$ for PWT; $F_{6,140} = 1.02$ for PWL; $^{*}P < 0.05$, $^{**}P < 0.01$, $^{***}P < 0.001$ versus the corresponding vehicle group.

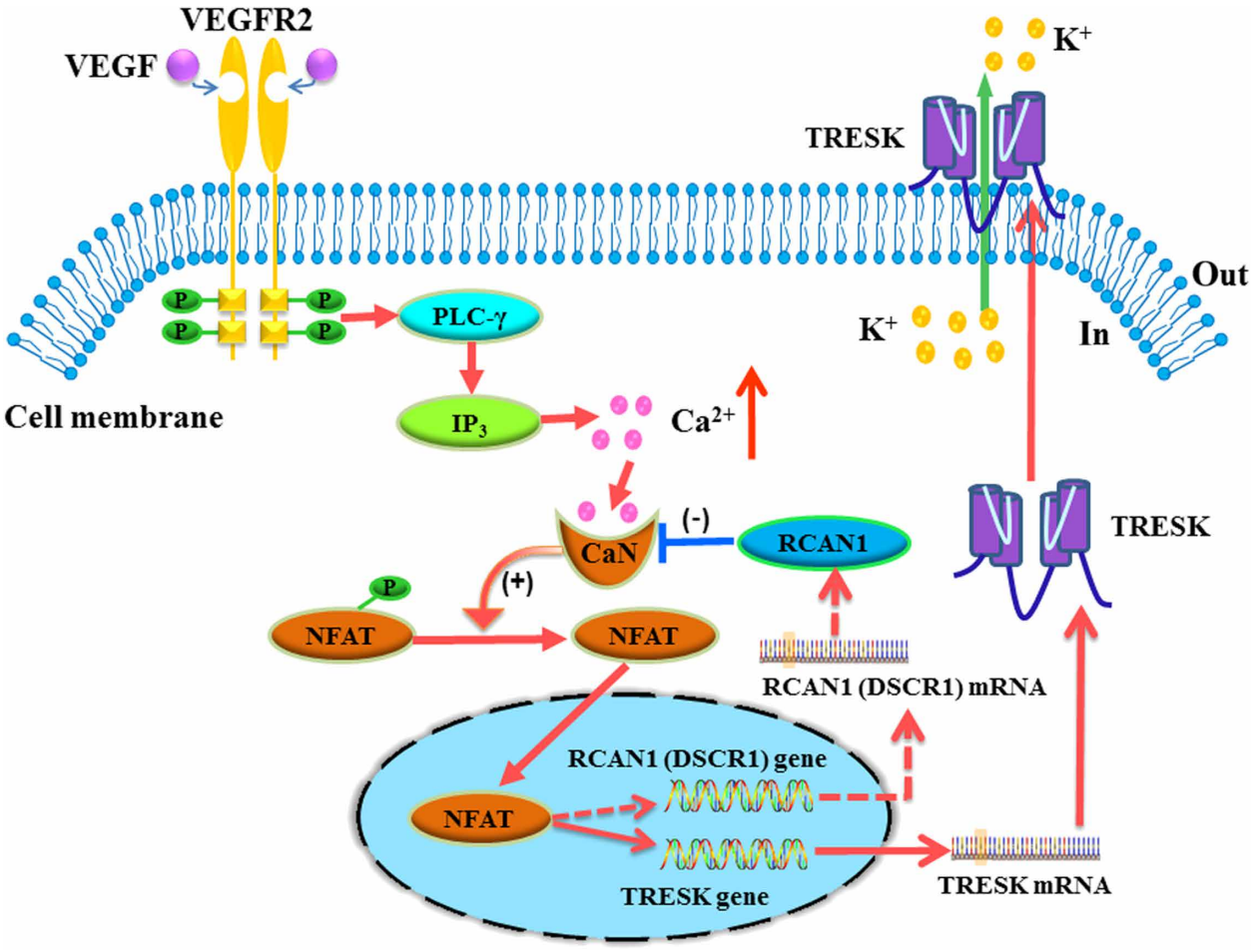

Fig. 8. The role of VEGF/calcineurin-NFAT/TRESK signaling in the development of bone cancer–induced pain. In the context of bone metastasis, the binding of VEGF to its receptor VEGFR2 may activate calcineurin, triggers NFAT translocation into nucleus, and consequently enhances the expression of NFAT targets, including the genes encoding TRESK and RCAN1, an endogenous calcineurin inhibitor. Enhancement of RCAN1 subsequently creates a negative feedback loop that inhibits calcineurin activity, thereby attenuating both the nuclear import of NFAT and the transactivation of its targets, including *TRESK*. The loss of TRESK abundance and, hence, activity in DRG neurons may result in neuronal hyperexcitability and peripheral sensitization, indicating a channel-mediated mechanism through which VEGF/VEGFR2 signaling contributes to bone cancer–induced pain.

Moreover, we presented additional evidence showing that knockdown of calcineurin by RNA interference reduced functional TRESK in DRG neurons and induced pain hypersensitivity in normal rats. These findings suggested that decreased calcineurin mediated the reduction of functional TRESK in DRG neurons, thereby contributing to the sensitization of nociceptive DRG neurons and metastasis-associated pain.

Calcineurin may act as a signaling mediator in pronociceptive pathways largely via its role in promoting the activation of NFAT (*20*). Activation of NFAT-mediated transcription has been implicated in the maintenance of pain in response to substance P in spinal neurons, whereas inhibiting NFAT suppresses several inflammatory pain (*49*, *50*). In agreement with these findings, we discovered that intrathecal administration of an NFAT inhibitor (VIVIT) could effectively abrogate the inhibitory effects of exogenous calcineurin on the tumor-induced reduction of TRESK in DRG neurons and pain hypersensitivity in bone lesion–bearing rats and that disrupting the calcineurin-NFAT interaction by VIVIT (*46*, *47*) produced a TRESK reduction in DRG neurons and pain hypersensitivity in normal rats. These data suggested that the disruption of the calcineurin-NFAT interaction is a possible cause for the functional suppression of TRESK by a decreased calcineurin in cancer rat DRG neurons.

In endothelial cells, binding of VEGF to VEGFR2 increases the endogenous calcineurin inhibitor RCAN1 (also called DSCR1), which triggers a negative feedback loop to inhibit the calcineurin's activity (*33*–*35*, *37*). VEGF could induce *DSCR1* gene expression, which encodes a regulatory protein that binds to calcineurin catalytic A subunit and acts as a regulator of the calcineurin-mediated signaling pathway. Apart from inhibiting the calcineurin's activity, VEGF also attenuates the elevation of calcineurin and nuclear NFATc3 proteins in isoproterenol-treated neonatal rat ventricular cardiomyocytes (*48*). In consistent with these findings, we documented that, with VEGF, treatment for cultured DRG neurons could decrease the calcineurin abundance and subsequently repressed the TRESK's expression and function. We proposed that a decreased calcineurin mediated the VEGF-induced TRESK reduction and the enhancement of neuronal excitability in cultured DRG neurons because additional calcineurin sufficiently inhibited these VEGF actions. In addition,

we found that disrupting the calcineurin-NFAT interaction with VIVIT also inhibited the VEGF-mediated reduction of TRESK protein and mRNA abundance, suggesting that the VEGF-mediated TRESK reduction is likely dependent on the calcineurin/NFAT signaling.

In conformity with previous observations showing that VEGF plays a role in the pathogenesis of neuropathic pain via VEGFR2 activation (*38*–*40*, *51*), we indeed found an increased abundance of both VEGF and VEGFR2 protein in cancer rat DRGs. Moreover, we found that intrathecal VEGF could decrease the calcineurin and TRESK abundance, enhanced DRG neuron excitability, and increased pain sensitivity in normal rats, whereas intrathecal VEGF antibody or VEGFR2 inhibitor (Ki8751) could reverse the tumor-induced reduction of both calcineurin and TRESK abundance, suppressed the DRG neuron hyperexcitability, and abrogated the tumor-induced pain hypersensitivity in bone metastasis models. These data suggested that activation of VEGF/VEGFR2 signaling is essential for the decreased calcineurin-mediated TRESK reduction and pain hypersensitivity in bone lesion–bearing rats. Our present data, together with previous findings (*32*–*35*, *44*), suggest that, under cancer conditions, the binding of VEGF to VEGFR2 may activate calcineurin (*52*, *53*), trigger NFAT translocated into the nucleus, and enhance the endogenous calcineurin inhibitor RCAN1 (DSCR1). Enhancement of RCAN1 subsequently creates a negative feedback loop to inhibit calcineurin activity, thereby attenuating NFAT nuclear import and the transactivation of its targets such as TRESK (*33*, *36*, *37*) (Fig. 8).

In conclusion, our data suggested that a reduction of functional TRESK channels in DRG neurons contributes to the sensitization of nociceptive sensory neurons and cancer pain development through enhancing neuronal excitability. Moreover, working as a positive regulator of TRESK, a decreased calcineurin likely mediates the reduction of functional TRESK channels in cancer rat DRG neurons. In addition, activation of VEGF/VEGFR2 signaling is required for the decreased calcineurin-mediated TRESK reduction and pain hypersensitivity in bone lesion–bearing rats. Thus, the decreased calcineurin-mediated TRESK reduction in DRG neurons via the activation of VEGF/VEGFR2 signaling may result in neuronal hyperexcitability and peripheral sensitization, thereby playing a crucial role in the pathogenesis of bone metastasis–induced pain.

MATERIALS AND METHODS

Animals

Adult Sprague-Dawley rats, weighing 200 to 220 g at the beginning of the experiments, were randomly allocated into groups. All animals were housed in separate cages, and the room was kept at 24° ± 1°C and 50 to 60% humidity under a 12-hour light/12-hour dark cycle with ad libitum access to food and water. All experimental procedures were carried out in accordance with the guidelines of the International Association for the Study of Pain (*54*) and were approved by the Animal Care and Use Committee of Peking University.

Reagents

Chemicals including Ki8751 (Selleck Chemicals), 11R-VIVIT (MedChem Express), lamotrigine (Sigma-Aldrich), and FK-506 (Sigma-Aldrich) were dissolved in dimethyl sulfoxide (DMSO; Sigma) to make a stock solution and stored at −20°C. The stock solution was subsequently diluted with sterile normal saline to make desired final concentrations immediately before administration. The final concentration of DMSO was less than 0.5%. Recombinant human calcineurin and rat $VEGF_{164}$ were purchased from Enzo Life Sciences (Farmingdale, NY) and R&D Systems (Minneapolis, MN), respectively. DAPI and toluidine blue dye were respectively obtained from Solarbio (Beijing, China) and Macklin (Shanghai, China). siRNA targeting rat TRESK (RSS328832) or calcineurin (53436) was obtained from Invitrogen (Carlsbad, CA) and GenePharma (Shanghai, China), respectively. Interfering peptide TAT-Ser and its control peptide TAT-Ala were synthesized from GL Biochem (Shanghai, China). Neutralizing peptides blocking the TRESK antibody were purchased from Alomone Labs (Jerusalem, Israel). Nucl-Cyto-Mem preparation kit was purchased from Applygen Technologies (Beijing, China). All other chemicals or reagents were obtained from Sigma-Aldrich except as mentioned in the text. Antibodies for all experiments in this study are listed in table S1.

Animal model of bone metastasis–associated pain

A rat model of pain induced by tumor metastasis to the bone was established by intratibial injection of syngeneic MRMT-1 rat mammary gland carcinoma cells as described in our previous studies (*55*, *56*). Briefly, after being anesthetized with 10% chloral hydrate [0.3 g/kg, intraperitoneal (ip)], the left tibia of rat was carefully exposed and a 23-gauge needle was inserted in the intramedullary canal of the bone. It was then removed and replaced with a long, thin blunt needle attached to a 10-μl Hamilton syringe containing the medium to be injected. A volume of 4 μl of MRMT-1 tumor cells (4×10^4) or vehicle (PBS) was injected into the tibial bone cavity. After injection, the site was sealed with bone wax, and the wound was finally closed. Any rats exhibiting motor deficiency or lack of pain hypersensitivity after tumor cell inoculation, as well as those that died during the experiments, were excluded from the study.

Drug administration

TRESK siRNA (2 μg) or an equal dose of scramble siRNA in a 10-μl mixture with in vivo jetPEI transfection reagent (Polyplus-transfection SA, Illkirch, France) was intrathecally administered to the normal rats once per day and continued for 2 days (see Fig. 3). FK-506 (20 μg in a 10-μl volume) or vehicle was intrathecally administered to the normal rats twice per day for two consecutive days (see figs. S8 and S10). Recombinant human calcineurin (10 enzyme units/μl) or saline in a 10-μl volume was intrathecally administered to the cancer rats on day 14 after tumor cell inoculation, once per day for two consecutive days (see Fig. 4). In some experiments, TRESK siRNA (2 μg in a 10-μl volume) or the scramble siRNA was intrathecally administered to the bone metastasis model rats on days 14 and 15 after surgery after calcineurin (10 enzyme units/μl × 10 μl) application (see fig. S12). Calcineurin siRNA (2 μg in a 10-μl volume) or the scramble siRNA was intrathecally delivered to the normal rats, once every 2 days, for 7 days (see fig. S13). 11R-VIVIT (100 μM × 10 μl) or vehicle was intrathecally administered to the normal rats once per day for seven consecutive days (see fig. S14). In bone metastasis model rats, the same dose of 11R-VIVIT was intrathecally administered to the animals on day 7 after tumor cell inoculation, once per day for seven consecutive days, and on day 6 after VIVIT injection, calcineurin (10 enzyme units/μl × 10 μl) was intrathecally applied to the bone lesion–bearing animals once per day for two consecutive days (see Fig. 5). Recombinant rat $VEGF_{164}$ (25 ng in a 10-μl volume) or vehicle was intrathecally administered to the normal rats twice per day for two consecutive days (see Fig. 6). Anti-VEGF antibody (300 ng/10 μl, once a day), or immunoglobulin G (IgG)

at an equal dose, was intrathecally applied to the cancer rats on day 14 after tumor cell inoculation (see fig. S16). Ki8751 (100 nM/10 μl, twice a day) or vehicle was intrathecally delivered to the bone metastasis model rats on day 14 after inoculation of the tumor cells (see Fig. 7).

Behavioral tests

All behavioral experiments thereafter were performed in a blinded fashion (the tester was blinded to treatment groups). Animals were randomly placed into treatment groups with 10 to 14 rats per treatment group per trial in consideration of the excluded ones, and the number for statistical analysis did not include the excluded rats.

Spontaneous pain-related behaviors were recorded as described elsewhere (*57*, *58*). Flinching and guarding were observed for 10 min during a resting state after a 30-min acclimation period. Flinching was defined as the lifting and rapid flexing of the ipsilateral hindpaw not associated with walking or movement. The number of flinches was recorded within the 10-min observation period. Guarding was characterized by fully retracting the ipsilateral hindlimb under the torso. The time the hindpaw was retracted during the 10-min period was recorded. Studies were performed in a blinded manner (the observer was blinded to all treatments).

Mechanical hypersensitivity, as a behavioral sign of bone cancer pain, was assessed by measuring 50% PWT as described in our previous reports (*59*, *60*). The 50% PWT in response to a series of von Frey filament (Stoelting, Wood Dale, IL) was determined by the up-and-down method (*61*). Eight von Frey filaments with about equal logarithmic incremental (0.224) bending forces were chosen (0.41*g*, 0.70*g*, 1.20*g*, 2.00*g*, 3.63*g*, 5.50*g*, 8.50*g*, and 15.10*g*). The 50% PWT was calculated using the following formula: 50% PWT (g) = $10^{[X_f+\kappa\delta]}$, where X_f is the value of the final von Frey filament used (in log units), κ is a value measured from the pattern of positive/negative response, and δ = 0.224, which is the average interval (in log units) between the von Frey filaments (*62*). If an animal did not respond to the highest von Frey filament, then the value was recorded as 15.10 g. In rats, the mechanical hypersensitivity is assessed by measuring the 50% PWT to von Frey filaments, and an allodynic rat is defined as that whose 50% PWT is less than 4.0 g (i.e., withdrawal in response to non-noxious tactile stimulus) (*63*).

Thermal hyperalgesia of the hindpaws was tested as described in our previous studies (*3*, *64*). Rats were allowed to acclimate for a minimum of 30 min before testing. Their PWL in response to radiant heat stimulation was measured. A maximal cutoff time of 30 s was used to prevent unnecessary tissue damage. The PWL was recorded and averaged over three trials at 5-min intervals.

Locomotor function was assessed with the inclined plate test, according to the method reported by Rivlin and Tator (*65*). Briefly, animals were placed crosswise to the long axis of an inclined plate. The initial angle of the inclined plate was 50°. The angle was then adjusted in 5° increments. The maximum angle of the plate on which the rat maintained its body position for 5 s without falling was determined. In this study, the inclined plate test was performed for all behavioral experiments in which the animals received intrathecal drugs.

Intrathecal catheterization

Intrathecal catheterization is a reliable approach for the delivery of drugs or vectors into the DRG of rats (*66*, *67*), and chronic lumbar catheterization of the spinal subarachnoid space in rodents offers several advantages for intrathecal delivery of drugs upon repeated administration (*68*–*70*). Therefore, intrathecal catheterization is well suited for long-term behavioral and pharmacological studies. Under chloral hydrate (0.3 g/kg, ip) anesthesia, implantation of an intrathecal catheter was performed as described in previous studies (*71*, *72*). Briefly, a PE-10 polyethylene catheter was implanted between the L5 and L6 vertebrae to reach the lumbar enlargement of the spinal cord. The correct intrathecal localization was confirmed by a tail flick or a paw retraction, by easy insertion of a catheter through the cannula, and occasionally by backflow of spinal fluid. The outer part of the catheter was plugged and fixed onto the skin upon closure of the wound. All surgical procedures were performed under sterile conditions. Rats showing neurological deficits after the catheter implantation were euthanized. In some experiments for intrathecal delivery of either lentivirus or drugs to cancer rats, the surgery for catheter placement was performed after tumor cell inoculation under the same anesthesia to avoid the animal being subjected to additional anesthesia. After recovery for 5 to 7 days, drugs or vectors were intrathecally injected via the implanted catheter in a 10-μl volume of solution (for lentivirus injection, 25 μl) followed by 10 μl of vehicle for flushing. Each injection lasted for at least 5 min. After an injection, the needle remained in situ for 2 min before being withdrawn.

After the experiments, a toluidine blue dye injection test was performed to verify the access of intrathecal injection to the DRG except for intrathecal delivery of lentivirus to the DRG, in which the expression of green fluorescent protein (GFP) in the DRG was assessed by immunofluorescence staining with anti-GFP and anti-TRESK. For the dye injection test, a 10-μl toluidine blue dye was intrathecally injected to rats, and the access of dye into DRG was validated at the end of the experiments (see fig. S4C).

Plasmid construction and lentivirus infection

The rTRESK-pcDNA3.1 plasmid was provided by X. Gasull (University of Barcelona, Barcelona, Spain). Construction and production of recombinant lentivirus expressing TRESK linked with ZsGreen (LV-TRESK) were completed by BioWit Technologies (Shenzhen, China) using pLVX-mCMV-ZsGreen vector, which contains GFP ZsGreen. Validation of the transfection efficiency and the cellular specificity of lentivirus infection was performed on primary cultured DRG neurons. Cultured DRG neurons on day 3 in vitro were exposed to virus for 48 hours at a multiplicity of infection (MOI). About 48 hours after viral infection, a transfection efficiency of lentivirus was routinely achieved as observed under fluorescence microscopy, and immunofluorescence staining with NeuN and ZsGreen was carried out to determine the cellular specificity of lentivirus infection (see fig. S4). For the in vivo studies, lentivirus, including LV-TRESK and its control LV-ZsGreen, was intrathecally administered to rats at a final titer of 4×10^8 transducing units/ml (in a 25-μl volume of solution), respectively. The lentivirus was intrathecally delivered to animals on day 7 after inoculation of PBS or tumor cells based on our previous findings (see Fig. 2) (*3*, *73*).

Primary culture and acute dissociation of DRG neurons

Primary cultures of DRG neurons were performed according to a method described previously (*74*). Briefly, rats (2 weeks old) were euthanized with ether, and DRGs were dissected from the lumbar spinal segments. The ganglia were digested with collagenase type IA (3 mg/ml; Sigma) for 45 min and 0.25% trypsin (type II-S, Sigma-Aldrich) for another 12 min at 37°C. After terminating the enzymatic

treatment by Dulbecco's modified Eagle's medium plus 10% fetal bovine serum, ganglia were dissociated with a polished Pasteur pipette, and the suspension of ganglia was sieved through a filter to remove debris and centrifuged at 800 rpm for 2 min. The resuspended cells were plated on 35-mm dishes coated with poly-D-lysine (0.5 mg/ml; Sigma-Aldrich), kept for 3 hours, and replaced with neurobasal growth medium containing B27 supplement, 0.5 mM L-glutamax (Sigma-Aldrich), penicillin (100 U/ml), and streptomycin (100 mg/ml). The cells were kept at 37°C in an incubator with 5% CO_2 and 95% air for 3 days before further treatment. Cultures were fed daily with neurobasal growth medium containing B27 supplement.

Acute dissociation of DRG neurons was performed as described in our previous reports (*55*, *73*). Briefly, neurons were isolated from the L4 and L5 DRGs of adult rats and were digested using the same procedure as described for primary cell culture above. The dissociated cells were used for patch-clamp recording within 3 to 8 hours of plating.

Immunofluorescence staining

To prepare DRG tissue samples for immunofluorescence analysis, deeply anesthetized rats were intracardially perfused with 50 ml of 0.1 M phosphate buffer (PB), followed by 500 ml of cold 4% paraformaldehyde [in 0.1 M PB (pH 7.4)]. After perfusion, the ipsilateral L4/5 DRG tissues were removed quickly, postfixed for 4 hours in the perfusion fixative, and cryoprotected in 30% sucrose (in 0.1 M PBS) overnight at 4°C. Serial frozen DRG sections (10 μm thick) were cut on a cryostat and thaw mounted on gelatin-coated slides for immunostaining processing. To prepare cultured HEK293 cells or cultured DRG neurons that were transfected with LV-TRESK (or LV-ZsGreen) or exposed to FK-506, the cells were rinsed for 5 min with PBS and fixed for 10 min with 4% paraformaldehyde in PBS at room temperature.

For immunostaining, the tissues or cultured cells were washed three times in PBS for 5 min each and blocked in 10% goat serum (in 0.1 M PBS) with 0.3% Triton X-100 for 1 hour at room temperature. Then, tissues or cultured cells were incubated with the respective primary antibody (see table S1) in PBS at 4°C overnight, which includes rabbit anti-rat TRESK (1:200), rabbit anti-mouse NeuN (1:200), mouse anti-pig glial fibrillary acidic protein (GFAP) (1:200), mouse anti-pig NF200 (1:200), mouse anti-rat calcitonin gene-related peptide (CGRP) (1:200), and rabbit anti-rat NFATc4 (1:300). For IB4 immunostaining, after three washes in PBS, the tissues were incubated with fluorescein isothiocyanate (FITC)–conjugated Bandeiraea simplicifolia isolectin B4 (IB4) (10 μg/ml) for 3 hours. Then, after three washes in PBS, tissues or cultured cells were incubated with the following appropriate secondary antibodies at room temperature for 1 hour: tetramethyl rhodamine isothiocyanate (TRITC)–labeled goat anti-rabbit IgG (1:200), fluorescein-5-isothiocyanate (FITC)–labeled goat anti-rabbit IgG (1:200), FITC-labeled goat anti-mouse IgG (1:200), or Alexa Fluor 647 goat anti-mouse IgG (1:200). In some experiments, the tissues or cultured cells were counterstained with the nuclear marker DAPI (100 ng/ml) carrying blue fluorescence for 10 min at room temperature. The tissues were mounted in Gel-Mount medium. Visualization of fluorescence signal was performed by confocal microscopy at excitation wavelengths of 488 nm (green), 543 nm (red), and 405 and 647 nm (blue). At least four fields per well or per section were analyzed to establish reproducibility.

Nuclear extraction

Cultured DRG neurons were lysed by homogenization with a Nucl-Cyto-Mem preparation kit (Applygen Technologies) according to the manufacturer's instructions with some modifications as previously described (*75*, *76*). The nuclear pellet was homogenized in ice-cold lysis buffer containing 50 mM tris (pH 8.0), 150 mM NaCl, 1% NP-40 (Sigma-Aldrich), 0.5% sodium deoxycholate (Sigma-Aldrich), 0.1% SDS, and protease inhibitor cocktail (Roche, Indianapolis, IN). The concentration of protein was measured with a bicinchoninic acid assay kit (Pierce, Rockford, IL), and the samples were subjected to SDS–polyacrylamide gel electrophoresis (PAGE).

Immunoprecipitation and Western blotting

Cultured DRG neurons or the dissected rat L4/5 DRGs were immediately homogenized in ice-cold lysis buffer containing 50 mM tris (pH 8.0), 150 mM NaCl, 1% NP-40 (Sigma-Aldrich), 0.5% sodium deoxycholate (Sigma-Aldrich), 0.1% SDS, 1% protease inhibitor cocktail, and 1% protein phosphatase inhibitor cocktails (Roche, Indianapolis, IN). After being rotated at 4°C for 1 hour, the homogenates were centrifuged at 12,000 rpm for 10 min to yield the total protein extract in the supernatant, and the supernatant was analyzed.

For immunoprecipitation, the sample containing 600 μg of protein was incubated with the anti-TRESK primary antibody (1:1000) at 4°C and gently shaken overnight. The immune complexes were collected with 30 μl of protein A/G agarose beads for 4 hours at 4°C. Immunoprecipitates were centrifuged at 3000 rpm for 5 min, and then the beads were washed six times and mixed with 800 μl of lysis buffer and centrifuged at 3000 rpm for 3 min. Sample loading buffer (2×) was mixed with the beads and boiled for 5 min to elute the precipitated TRESK protein. These samples, almost all of which were the precipitated TRESK protein, were subjected to SDS-PAGE and transferred onto a polyvinylidene difluoride filter (PVDF) membrane (Bio-Rad, Hercules, CA). The blotting analysis was performed by repeated stripping and successive probing with the following antibodies: anti-phosphoserine (1:300) and anti-TRESK (1:1000).

For Western blotting, the sample containing 60 μg of protein was denatured and then separated through SDS-PAGE using 10 to 12% separating gels and transferred to a PVDF membrane (Bio-Rad, Hercules, CA). The membranes were blocked with 5% nonfat milk in TBST [20 mM tris-HCl (pH 7.5), 150 mM NaCl, and 0.05% Tween 20] for 60 min at room temperature and then incubated with the following primary antibodies at 4°C overnight: anti-TRESK (1:1000), anti-calcineurin (1:1000), anti-VEGF (1:1000), anti-VEGFR2 (1:200), anti-phosphoserine (1:300), anti-NFATc4 (1:300), anti–acetyl-histone H3 (1:300), and anti–β-actin (1:2000). The blots were washed in TBST and then were incubated in horseradish peroxidase–conjugated secondary antibody (1:2000, goat anti-rabbit/mouse or rabbit anti-goat IgG). Protein bands were visualized using an enhanced chemiluminescence detection kit (Pierce) followed by autoradiography using Hyperfilm MP (Santa Cruz Biotechnology). The band was quantified with a computer-assisted imaging analysis system (ImageJ, NIH).

Detection of phosphorylated TRESK abundance was carried out by using co-immunoprecipitation (co-IP) combined with Western blot: Because no commercial antibody against phosphorylated TRESK at specific serine residue is available, we therefore performed co-IP combined with Western blot to detect the phosphorylated TRESK abundance at the gross serine residues (pTRESKser). The detailed protocol was carried out according to the methods as previously described (*77*, *78*). First, we obtained the total protein from cultured DRG neurons or the dissected rat L4/5 DRGs and performed co-IP

by incubating the anti-TRESK antibody with the total protein. This step aimed to precipitate the TRESK protein from the total protein. Second, we used the A/G agarose beads to pull down the TRESK protein. After the beads were boiled, we obtained the protein samples, almost all of which were the precipitated TRESK protein. Last, we performed Western blot analysis by incubating the anti-phosphoserine antibody with the precipitated TRESK protein. Therefore, the bands we obtained from the Western blot could be considered as the phosphorylated TRESK abundance at the gross serine residues (pTRESKser).

Neutralizing peptide blocking experiment

The specificity validation of anti-TRESK was carried out via a neutralizing peptide blocking experiment using a specific blocking peptide targeting anti-TRESK antibody. Briefly, before proceeding with the immunoblot protocol, the antibody was neutralized by coincubation with a specific blocking peptide that corresponds to the epitope recognized by the antibody. The antibody that was bound to the blocking peptide was no longer available to bind to the epitope present in the protein. The neutralized antibody was then used side by side with the antibody alone, and the immunoblot from the blocked antibody was compared with that from the antibody alone. The specific immunoblot signal was blocked by preincubation with a specific blocking peptide but not by a control peptide IgG. The specificity of the anti-TRESK antibody was determined by specific inhibition of TRESK immunoblot after coincubation with a specific blocking peptide targeting the TRESK antibody.

RNA extraction and RT-qPCR

Total RNA was extracted from the rat L4/L5 DRGs with TRIzol reagent (Life Technologies). Reverse transcription was performed with oligo deoxythymidine (oligo-dT) primers and Moloney murine leukemia virus reverse transcriptase (Promega) according to the manufacturer's protocol. PCR primer sequences are listed in table S2. RT-qPCR was performed with GoTaq qPCR Master Mix (Promega) and an ABI 7500 Fast Real-Time PCR Detection System (Applied Biosystems). Briefly, a 20-μl PCR reaction that included 1 μl of complementary DNA, 10 μl of GoTaq qPCR Master Mix, and 0.2 μM of each primer was used and adjusted to the final volume with double distilled H_2O (ddH_2O). β-Actin in parallel for each run was used as an internal control. The reactions were set up on the basis of the manufacturer's protocol. PCR conditions were incubation at 95°C for 3 min followed by 40 cycles of thermal cycling (10 s at 95°C, 20 s at 58°C, and 10 s at 72°C). The relative expression ratio of mRNA was quantified via the $2^{-(\Delta\Delta Ct)}$ method.

Construction of interfering peptide

To determine whether the action of calcineurin is mediated via intracellular dephosphorylation of TRESK channel, we constructed a specific interfering peptide TAT-Ser (sequence: RKKRRQRRR-{pSercN{pSer}CPELVLGRL{pSer}C{pSer}IL{pSer}NLDE), which is composed of 22 amino acids of the TRESK regulatory sites including the calcineurin-mediated dephosphorylation sites, serine 252, serine 262, serine 264, and serine 267, thereby disrupting endogenous phosphorylation/dephosphorylation of TRESK. The control peptide TAT-Ala (sequence: RKKRRQRRR-ANACPELVLGRLACAILANLDE) was designed with alanine to replace serine 252, serine 262, serine 264, and serine 267. Cultured DRG neurons on day 3 in vitro were exposed to TAT peptide (10 μg in a 2-μl volume) for 12 hours before application of calcineurin and then exposed to the same dose of TAT peptide associated with recombinant calcineurin (10 enzyme units/μl) for another 24 hours.

Alteration of TRESK abundance in the DRG was assayed by Western blotting. Whole-cell patch-clamp recording was performed on drug-treated DRG neurons to examine alterations of TRESK currents and DRG neuron excitability (see fig. S9).

siRNA preparation and screening

Targeted siRNAs were applied to knock down the abundance of TRESK and calcineurin. Briefly, siRNAs (three each) targeting rat TRESK or calcineurin mRNA were designed and synthesized by Invitrogen and GenePharma, respectively. Sequences are listed in table S3. Knockdown efficiency was determined by RT-qPCR and Western blotting. The preliminary experiments showed that intrathecal injection of TRESK siRNA3 (2 μg in a 10-μl volume) or calcineurin siRNA1 (2 μg in a 10-μl volume) could significantly inhibit the abundance of their respective protein in the DRG. Hence, the synthesized TRESK siRNA3 and calcineurin siRNA1 were chosen for the present study.

Electrophysiology

Whole-cell patch-clamp recordings were performed on acutely dissociated or primary cultured DRG neurons at room temperature using an EPC-10 amplifier with Patch-Master software (HEKA, Freiburg, Germany). The recording pipette had a resistance of 4 to 8 megohms when filled with an internal solution containing 140 mM KCl, 1 mM EGTA (ethylene glycol tetraacetic acid), 5 mM Hepes, 2 mM $MgCl_2$, and 1 mM Na_2ATP, adjusted to pH 7.3 with KOH. The external solution contained 135 mM NaCl, 5.4 mM KCl, 1.8 mM $CaCl_2$, 1 mM $MgCl_2$, 10 mM glucose, and 5 mM Hepes, adjusted to pH 7.4 with NaOH. Drugs were prepared in the external solution and delivered by an RSC-200 rapid solution changer system (Bio-Logic Science Instruments, Grenoble, France). Membrane currents and APs were measured with both pipette and membrane capacitance cancellation, filtered at 2 kHz, and digitized at 10 kHz. RMP was measured immediately after rupture of the cell membrane in whole-cell patch mode. In this study, IB4-labeled, small-sized DRG neurons were performed by electrophysiological studying. In some experiments, the $IB4^-$, small DRG neurons were also studied. The FITC-labeled lectin IB4 was used as a live cell marker to identify nociceptive neurons (*79*). Somata of small-sized DRG neurons were defined by their diameters (≤30 μm) and membrane capacitance (C_m) (≤28.3 pF) as described in previous studies (*56*, *80*).

Under current-clamp recording, the cells were held at 0 pA, and the firing threshold of DRG neurons was first measured by a series of 100-ms depolarizing current injection in 5-pA steps from 0 pA to elicit the first AP. To further examine the firing properties of neurons, a large depolarizing current (500 ms, 2.5-fold AP threshold) was delivered to elicit the cell generating sufficient firing. In this study, we measured RMP, rheobase (the current threshold for eliciting an AP), and frequency of AP to evaluate the intrinsic electrophysiological properties of cells.

Under voltage-clamp recording, cells were clamped at −70 mV, and series resistance was compensated from 75 to 90%. The membrane capacitance was read from the amplifier by Patch-Master software (HEKA) to determine the size of cells and to calculate the current density. In this study, two protocols were used to elicit and measure TRESK currents. First, a ramp voltage protocol from −120 to +60 mV was applied to elicit total background currents (IK_{BG}), which include TRESK current, and the current amplitude was measured at +60 mV

(*5*, *7*). Then, a step voltage protocol was designed to minimize activation of voltage-gated transient K^+ currents (*5*) and to inactivate both the fast tetrodotoxin-resistant Na^+ currents and high-voltage–activated Ca^{2+} currents, which has been shown to be able to elicit a standing outward current (IK_{SO}), the majority of TRESK-containing IK_{SO} (*8*, *9*, *81*). Initially, the membrane potential was depolarized from a holding potential of −70 to −25 mV for 500 ms and subsequently hyperpolarized to −135 mV within 1 s. Current amplitude was measured after 500 ms at the end of the depolarizing step (−25 mV) (*5*, *7*–*9*). One of the TRESK inhibitors, lamotrigine (100 μM), was applied to dissect current through TRESK channels as described in previous studies (*7*–*9*, *42*). It has been shown that this dose of lamotrigine inhibits TRESK currents by 50% (*7*, *42*). In addition, the specificity of lamotrigine has also been validated systematically in previous studies (*42*, *82*). Sipatrigine, a derivative of lamotrigine, markedly inhibited human TREK-1, whereas lamotrigine weakly inhibited it (*82*). In COS-7 cells expressing TREK-2 or TRESK, fluoxetine (an antidepressant) inhibited both TRESK and TREK-2, while lamotrigine inhibited only TRESK, indicating that lamotrigine specifically acts on TRESK (*42*). The mechanism by which lamotrigine induced TRESK inhibition is proposed to be regulated by blockade of calcium influx and glutamate release (*42*, *83*). Origin software 8.5 (OriginLab Corporation, Northampton, MA) was used for data analysis.

Statistical analysis

All data were expressed as means ± SEM. One-way ANOVA followed by Tukey's multiple comparison test or two-way ANOVA followed by Bonferroni post hoc test was used for multiple comparison. Two-tailed unpaired Student's *t* test was used for the comparison of the mean values between two groups. All data were subjected to a normal distribution test, and only the data with a normal distribution were subjected to *t* test or ANOVA. The correlation between TRESK protein abundance and spontaneous pain behaviors (flinching and guarding) after tumor cell inoculation was analyzed. Differences with $P < 0.05$ were considered statistically significant. Statistical analyses were performed with GraphPad Prism 7 for Windows (GraphPad Software, La Jolla, CA).

SUPPLEMENTARY MATERIALS

www.sciencesignaling.org/cgi/content/full/11/552/eaao5150/DC1

Fig. S1. Distribution and alteration of TRESK channels in ipsilateral L4/5 DRG neurons of bone lesion–bearing rats.

Fig. S2. TRESK antibody validation in HEK293 cells.

Fig. S3. Reduction of TRESK-containing currents in $IB4^-$ DRG neurons of bone lesion–bearing rats.

Fig. S4. Augmented TRESK staining in DRG neurons upon intrathecal administration of lentiviral TRESK.

Fig. S5. Effects of TRESK overexpression on the tumor-induced TRESK repression and neuronal hyperexcitability in $IB4^-$ DRG neurons from bone lesion–bearing rats.

Fig. S6. Effects of intrathecal injection of TRESK siRNA on the expression of other K2P family members in bilateral L4/5 DRGs from normal rats.

Fig. S7. Effects of TRESK knockdown on neuronal excitability in $IB4^-$ DRGs from normal rats.

Fig. S8. Effects of calcineurin inhibition on the abundance of phosphorylated TRESK in DRG neurons.

Fig. S9. Effects of interfering peptide TAT-Ser on calcineurin-induced alterations of functional TRESK abundance and neuronal excitability in cultured DRG neurons.

Fig. S10. Effects of FK-506 treatment on functional TRESK abundance and neuronal excitability in cultured DRGs and on pain sensitivity in normal rats.

Fig. S11. The subcellular distribution of NFAT in cultured DRG neurons upon treatment with FK-506.

Fig. S12. Effects of TRESK knockdown on calcineurin-modulated DRG neuron excitability and pain sensitivity in bone lesion–bearing rats.

Fig. S13. Effects of intrathecal injection of calcineurin siRNA on functional TRESK abundance, DRG neuron excitability, and pain sensitivity in normal rats.

Fig. S14. Effects of intrathecal injection of NFAT inhibitor peptide VIVIT on functional TRESK abundance, DRG neuron excitability, and pain sensitivity in normal rats.

Fig. S15. Effects of VEGF treatment on calcineurin and TRESK abundance, TRESK-mediated currents, and the neuronal excitability in cultured DRG neurons.

Fig. S16. Effects of VEGF antibody on calcineurin and TRESK abundance, DRG neuron excitability, and pain hypersensitivity in bone lesion–bearing rats.

Table S1. Antibodies.

Table S2. PCR primer sequences.

Table S3. siRNA nucleotide sequences.

REFERENCES AND NOTES

1. C. M. Kane, P. Hoskin, M. I. Bennett, Cancer induced bone pain. *BMJ* **350**, *h315* (2015).
2. J. Zhao, H.-L. Pan, T.-T. Li, Y.-Q. Zhang, J.-Y. Wei, Z.-Q. Zhao, The sensitization of peripheral C-fibers to lysophosphatidic acid in bone cancer pain. *Life Sci.* **87**, 120–125 (2010).
3. Q. Zheng, D. Fang, J. Cai, Y. Wan, J. S. Han, G. G. Xing, Enhanced excitability of small dorsal root ganglion neurons in rats with bone cancer pain. *Mol. Pain* **8**, 24–28 (2012).
4. D. Kang, D. Kim, TREK-2 (K_{2P}10.1) and TRESK (K_{2P}18.1) are major background K^+ channels in dorsal root ganglion neurons. *Am. J. Physiol. Cell Physiol.* **291**, C138–C146 (2006).
5. T. Dobler, A. Springauf, S. Tovornik, M. Weber, A. Schmitt, R. Sedlmeier, E. Wischmeyer, F. Döring, TRESK two-pore-domain K^+ channels constitute a significant component of background potassium currents in murine dorsal root ganglion neurones. *J. Physiol.* **585**, 867–879 (2007).
6. P. Enyedi, G. Czirják, Properties, regulation, pharmacology, and functions of the K_{2p} channel, TRESK. *Pflugers Arch.* **467**, 945–958 (2015).
7. A. Tulleuda, B. Cokic, G. Callejo, B. Saiani, J. Serra, X. Gasull, TRESK channel contribution to nociceptive sensory neurons excitability: Modulation by nerve injury. *Mol. Pain* **7**, 30–37 (2011).
8. P. Liu, Z. Xiao, F. Ren, Z. Guo, Z. Chen, H. Zhao, Y.-Q. Cao, Functional analysis of a migraine-associated TRESK K^+ channel mutation. *J. Neurosci.* **33**, 12810–12824 (2013).
9. Z. Guo, Y.-Q. Cao, Over-expression of TRESK K^+ channels reduces the excitability of trigeminal ganglion nociceptors. *PLOS ONE* **9**, e87029 (2014).
10. S. Kollert, B. Dombert, F. Döring, E. Wischmeyer, Activation of TRESK channels by the inflammatory mediator lysophosphatidic acid balances nociceptive signalling. *Sci. Rep.* **5**, 12548 (2015).
11. B. Marsh, C. Acosta, L. Djouhri, S. N. Lawson, Leak K^+ channel mRNAs in dorsal root ganglia: Relation to inflammation and spontaneous pain behaviour. *Mol. Cell. Neurosci.* **49**, 375–386 (2012).
12. J. Zhou, C.-X. Yang, J.-Y. Zhong, H.-B. Wang, Intrathecal *TRESK* gene recombinant adenovirus attenuates spared nerve injury-induced neuropathic pain in rats. *Neuroreport* **24**, 131–136 (2013).
13. G. Czirják, P. Enyedi, Targeting of calcineurin to an NFAT-like docking site is required for the calcium-dependent activation of the background K^+ channel, TRESK. *J. Biol. Chem.* **281**, 14677–14682 (2006).
14. G. Czirják, Z. E. Tóth, P. Enyedi, The two-pore domain K^+ channel, TRESK, is activated by the cytoplasmic calcium signal through calcineurin. *J. Biol. Chem.* **279**, 18550–18558 (2004).
15. G. Czirják, D. Vuity, P. Enyedi, Phosphorylation-dependent binding of 14-3-3 proteins controls TRESK regulation. *J. Biol. Chem.* **283**, 15672–15680 (2008).
16. A. Mathie, E. L. Veale, Two-pore domain potassium channels: Potential therapeutic targets for the treatment of pain. *Pflugers Arch.* **467**, 931–943 (2015).
17. G. Czirják, P. Enyedi, The LQLP calcineurin docking site is a major determinant of the calcium-dependent activation of human TRESK background K^+ channel. *J. Biol. Chem.* **289**, 29506–29518 (2014).
18. I. M. Mansuy, Calcineurin in memory and bidirectional plasticity. *Biochem. Biophys. Res. Commun.* **311**, 1195–1208 (2003).
19. R. D. Groth, R. L. Dunbar, P. G. Mermelstein, Calcineurin regulation of neuronal plasticity. *Biochem. Biophys. Res. Commun.* **311**, 1159–1171 (2003).
20. H. S. Smith, Calcineurin as a nociceptor modulator. *Pain Physician* **12**, E309–E318 (2009).
21. G. Miletic, J. A. Lippitt, K. M. Sullivan, V. Miletic, Loss of calcineurin in the spinal dorsal horn contributes to neuropathic pain, and intrathecal administration of the phosphatase provides prolonged analgesia. *Pain* **154**, 2024–2033 (2013).
22. G. Miletic, K. M. Sullivan, A. M. K. Dodson, J. A. Lippitt, J. A. Schneider, V. Miletic, Changes in calcineurin message, enzyme activity and protein content in the spinal dorsal horn are associated with chronic constriction injury of the rat sciatic nerve. *Neuroscience* **188**, 142–147 (2011).
23. G. Miletic, J. L. Hermes, G. L. Bosscher, B. M. Meier, V. Miletic, Protein kinase C gamma-mediated phosphorylation of GluA1 in the postsynaptic density of spinal dorsal horn neurons accompanies neuropathic pain, and dephosphorylation by calcineurin is associated with prolonged analgesia. *Pain* **156**, 2514–2520 (2015).
24. D.-Y. Huang, B.-W. Yu, Q.-W. Fan, Roles of TRESK, a novel two-pore domain K^+ channel, in pain pathway and general anesthesia. *Neurosci. Bull.* **24**, 166–172 (2008).

25. S. Ishida, M. Kato, T. Fujita, Y. Funahashi, N. Sassa, Y. Matsukawa, Y. Yoshino, T. Yamamoto, T. Katsuno, S. Maruyama, M. Gotoh, Calcineurin inhibitor–induced pain syndrome in abo-incompatible living kidney transplantation: A case report. *Transplant. Proc.* **49**, 163–166 (2017).
26. W. H. Grotz, M. K. Breitenfeldt, S. W. Braune, K. H. Allmann, T. M. Krause, J. A. Rump, P. J. Schollmeyer, Calcineurin-inhibitor induced pain syndrome (CIPS): A severe disabling complication after organ transplantation. *Transpl. Int.* **14**, 16–23 (2001).
27. S. Sahay, K. McBennett, T. Sheers, Calcineurin-inhibitor induced pain syndrome in a lung transplant patient. *Transpl. Int.* **26**, e71–e73 (2013).
28. Y. Noda, K. Kodama, T. Yasuda, S. Takahashi, Calcineurin-inhibitor-induced pain syndrome after bone marrow transplantation. *J. Anesth.* **22**, 61–63 (2008).
29. S.-R. Chen, Y.-M. Hu, H. Chen, H.-L. Pan, Calcineurin inhibitor induces pain hypersensitivity by potentiating pre- and postsynaptic NMDA receptor activity in spinal cords. *J. Physiol.* **592**, 215–227 (2014).
30. Y.-M. Hu, S.-R. Chen, H. Chen, H.-L. Pan, Casein kinase II inhibition reverses pain hypersensitivity and potentiated spinal *N*-methyl-D-aspartate receptor activity caused by calcineurin inhibitor. *J. Pharmacol. Exp. Ther.* **349**, 239–247 (2014).
31. E. Prommer, Calcineurin-inhibitor pain syndrome. *Clin. J. Pain* **28**, 556–559 (2012).
32. T. Minami, Calcineurin-NFAT activation and DSCR-1 auto-inhibitory loop: How is homoeostasis regulated? *J. Biochem.* **155**, 217–226 (2014).
33. Y.-G. Yao, E. J. Duh, VEGF selectively induces Down syndrome critical region 1 gene expression in endothelial cells: A mechanism for feedback regulation of angiogenesis? *Biochem. Biophys. Res. Commun.* **321**, 648–656 (2004).
34. B. A. Hesser, X. H. Liang, G. Camenisch, S. Yang, D. A. Lewin, R. Scheller, N. Ferrara, H.-P. Gerber, Down syndrome critical region protein 1 (DSCR1), a novel VEGF target gene that regulates expression of inflammatory markers on activated endothelial cells. *Blood* **104**, 149–158 (2004).
35. K. Holmes, E. Chapman, V. See, M. J. Cross, VEGF stimulates RCAN1.4 expression in endothelial cells via a pathway requiring Ca^{2+}/calcineurin and protein kinase C-δ. *PLOS ONE* **5**, e11435 (2010).
36. E. Cano, A. Canellada, T. Minami, T. Iglesias, J. M. Redondo, Depolarization of neural cells induces transcription of the Down syndrome critical region 1 isoform 4 via a calcineurin/nuclear factor of activated T cells-dependent pathway. *J. Biol. Chem.* **280**, 29435–29443 (2005).
37. T. Minami, K. Horiuchi, M. Miura, M. R. Abid, W. Takabe, N. Noguchi, T. Kohro, X. Ge, H. Aburatani, T. Hamakubo, T. Kodama, W. C. Aird, Vascular endothelial growth factor- and thrombin-induced termination factor, Down syndrome critical region-1, attenuates endothelial cell proliferation and angiogenesis. *J. Biol. Chem.* **279**, 50537–50554 (2004).
38. J. Lin, G. Li, X. Den, C. Xu, S. Liu, Y. Gao, H. Liu, J. Zhang, X. Li, S. Liang, VEGF and its receptor-2 involved in neuropathic pain transmission mediated by $P2X_{2/3}$ receptor of primary sensory neurons. *Brain Res. Bull.* **83**, 284–291 (2010).
39. R. P. Hulse, N. Beazley-Long, J. Hua, H. Kennedy, J. Prager, H. Bevan, Y. Qiu, E. S. Fernandes, M. V. Gammons, K. Ballmer-Hofer, A. C. Gittenberger de Groot, A. J. Churchill, S. J. Harper, S. D. Brain, D. O. Bates, L. F. Donaldson, Regulation of alternative VEGF-A mRNA splicing is a therapeutic target for analgesia. *Neurobiol. Dis.* **71**, 245–259 (2014).
40. O. Nesic, L. M. Sundberg, J. J. Herrera, V. U. L. Mokkapati, J. Lee, P. A. Narayana, Vascular endothelial growth factor and spinal cord injury pain. *J. Neurotrauma* **27**, 1793–1803 (2010).
41. D. Selvaraj, V. Gangadharan, C. W. Michalski, M. Kurejova, S. Stösser, K. Srivastava, M. Schweizerhof, J. Waltenberger, N. Ferrara, P. Heppenstall, M. Shibuya, H. G. Augustin, R. Kuner, A functional role for vegfr1 expressed in peripheral sensory neurons in cancer pain. *Cancer Cell* **27**, 780–796 (2015).
42. D. Kang, G.-T. Kim, E.-J. Kim, J.-H. La, J.-S. Lee, E.-S. Lee, J.-Y. Park, S.-G. Hong, J. Han, Lamotrigine inhibits TRESK regulated by G-protein coupled receptor agonists. *Biochem. Biophys. Res. Commun.* **367**, 609–615 (2008).
43. C. B. Klee, H. Ren, X. Wang, Regulation of the calmodulin-stimulated protein phosphatase, calcineurin. *J. Biol. Chem.* **273**, 13367–13370 (1998).
44. M. J. Kipanyula, W. H. Kimaro, P. F. Seke Etet, The emerging roles of the calcineurin-nuclear factor of activated T-lymphocytes pathway in nervous system functions and diseases. *J. Aging Res.* **2016**, 5081021 (2016).
45. S. Martinez-Martinez, J. M. Redondo, Inhibitors of the calcineurin/NFAT pathway. *Curr. Med. Chem.* **11**, 997–1007 (2004).
46. J. Aramburu, M. B. Yaffe, C. López-Rodríguez, L. C. Cantley, P. G. Hogan, A. Rao, Affinity-driven peptide selection of an NFAT inhibitor more selective than cyclosporin A. *Science* **285**, 2129–2133 (1999).
47. H. Noguchi, M. Matsushita, T. Okitsu, A. Moriwaki, K. Tomizawa, S. Kang, S.-T. Li, N. Kobayashi, S. Matsumoto, K. Tanaka, N. Tanaka, H. Matsui, A new cell-permeable peptide allows successful allogeneic islet transplantation in mice. *Nat. Med.* **10**, 305–309 (2004).
48. B. Cai, X. Tan, Y. Zhang, X. Li, X. Wang, J. Zhu, Y. Wang, F. Yang, B. Wang, Y. Liu, C. Xu, Z. Pan, N. Wang, B. Yang, Y. Lu, Mesenchymal stem cells and cardiomyocytes interplay to prevent myocardial hypertrophy. *Stem Cells Transl. Med.* **4**, 1425–1435 (2015).
49. V. S. Seybold, L. G. Coicou, R. D. Groth, P. G. Mermelstein, Substance P initiates NFAT-dependent gene expression in spinal neurons. *J. Neurochem.* **97**, 397–407 (2006).
50. M. A. Sama, D. M. Mathis, J. L. Furman, H. M. Abdul, I. A. Artiushin, S. D. Kraner, C. M. Norris, Interleukin-1β-dependent signaling between astrocytes and neurons depends critically on astrocytic calcineurin/NFAT activity. *J. Biol. Chem.* **283**, 21953–21964 (2008).
51. N. Kiguchi, Y. Kobayashi, Y. Kadowaki, Y. Fukazawa, F. Saika, S. Kishioka, Vascular endothelial growth factor signaling in injured nerves underlies peripheral sensitization in neuropathic pain. *J. Neurochem.* **129**, 169–178 (2014).
52. K. Holmes, O. L. Roberts, A. M. Thomas, M. J. Cross, Vascular endothelial growth factor receptor-2: Structure, function, intracellular signalling and therapeutic inhibition. *Cell. Signal.* **19**, 2003–2012 (2007).
53. M. J. Cross, J. Dixelius, T. Matsumoto, L. Claesson-Welsh, VEGF-receptor signal transduction. *Trends Biochem. Sci.* **28**, 488–494 (2003).
54. M. Zimmermann, Ethical guidelines for investigations of experimental pain in conscious animals. *Pain* **16**, 109–110 (1983).
55. D. Fang, L.-Y. Kong, J. Cai, S. Li, X.-D. Liu, J.-S. Han, G.-G. Xing, IL-6-mediated functional up-regulation of TRPV1 receptors in DRG neurons via the activation of JAK/PI3K signaling pathway: Roles in the development of bone cancer pain in a rat model. *Pain* **156**, 1124–1144 (2015).
56. Q. Zheng, D. Fang, M. Liu, J. Cai, Y. Wan, J.-S. Han, G.-G. Xing, Suppression of KCNQ/M (Kv7) potassium channels in dorsal root ganglion neurons contributes to the development of bone cancer pain in a rat model. *Pain* **154**, 434–448 (2013).
57. A. N. Lozano-Ondoua, C. Wright, A. Vardanyan, T. King, T. M. Largent-Milnes, M. Nelson, J. M. Jimenez-Andrade, P. W. Mantyh, T. W. Vanderah, A cannabinoid 2 receptor agonist attenuates bone cancer-induced pain and bone loss. *Life Sci.* **86**, 646–653 (2010).
58. T. E. King, S. C. Pawar, L. Majuta, I. C. Sroka, D. Wynn, M. C. Demetriou, R. B. Nagle, F. Porreca, A. E. Cress, The role of alpha 6 integrin in prostate cancer migration and bone pain in a novel xenograft model. *PLOS ONE* **3**, e3535 (2008).
59. X. Ding, J. Cai, S. Li, X.-D. Liu, Y. Wan, G.-G. Xing, BDNF contributes to the development of neuropathic pain by induction of spinal long-term potentiation via SHP2 associated GluN2B-containing NMDA receptors activation in rats with spinal nerve ligation. *Neurobiol. Dis.* **73**, 428–451 (2015).
60. H. Jiang, D. Fang, L.-Y. Kong, Z.-R. Jin, J. Cai, X.-J. Kang, Y. Wan, G.-G. Xing, Sensitization of neurons in the central nucleus of the amygdala via the decreased GABAergic inhibition contributes to the development of neuropathic pain-related anxiety-like behaviors in rats. *Mol. Brain* **7**, 72 (2014).
61. S. R. Chaplan, F. W. Bach, J. W. Pogrel, J. M. Chung, T. L. Yaksh, Quantitative assessment of tactile allodynia in the rat paw. *J. Neurosci. Methods* **53**, 55–63 (1994).
62. W. J. Dixon, Efficient analysis of experimental observations. *Annu. Rev. Pharmacol. Toxicol.* **20**, 441–462 (1980).
63. M. Zimmermann, Pathobiology of neuropathic pain. *Eur. J. Pharmacol.* **429**, 23–37 (2001).
64. X.-D. Liu, J.-J. Yang, D. Fang, J. Cai, Y. Wan, G.-G. Xing, Functional upregulation of nav1.8 sodium channels on the membrane of dorsal root ganglia neurons contributes to the development of cancer-induced bone pain. *PLOS ONE* **9**, e114623 (2014).
65. A. S. Rivlin, C. H. Tator, Objective clinical assessment of motor function after experimental spinal cord injury in the rat. *J. Neurosurg.* **47**, 577–581 (1977).
66. C. Towne, M. Pertin, A. T. Beggah, P. Aebischer, I. Decosterd, Recombinant adeno-associated virus serotype 6 (rAAV2/6)-mediated gene transfer to nociceptive neurons through different routes of delivery. *Mol. Pain* **5**, 52 (2009).
67. G. Li, F. Ma, Y. Gu, L.-Y. M. Huang, Analgesic tolerance of opioid agonists in mutant mu-opioid receptors expressed in sensory neurons following intrathecal plasmid gene delivery. *Mol. Pain* **9**, 63 (2013).
68. L. Gendron, A. L. Lucido, F. Mennicken, D. O'Donnell, J. P. Vincent, T. Stroh, A. Beaudet, Morphine and pain-related stimuli enhance cell surface availability of somatic delta-opioid receptors in rat dorsal root ganglia. *J. Neurosci.* **26**, 953–962 (2006).
69. W.-P. Wu, X.-J. Xu, J.-X. Hao, Chronic lumbar catheterization of the spinal subarachnoid space in mice. *J. Neurosci. Methods* **133**, 65–69 (2004).
70. L. Jasmin, P. T. Ohara, Long-term intrathecal catheterization in the rat. *J. Neurosci. Methods* **110**, 81–89 (2001).
71. S.-J. Geng, F.-F. Liao, W.-H. Dang, X. Ding, X.-D. Liu, J. Cai, J.-S. Han, Y. Wan, G. G. Xing, Contribution of the spinal cord BDNF to the development of neuropathic pain by activation of the NR2B-containing NMDA receptors in rats with spinal nerve ligation. *Exp. Neurol.* **222**, 256–266 (2010).
72. X.-X. Qu, J. Cai, M.-J. Li, Y.-N. Chi, F.-F. Liao, F.-Y. Liu, Y. Wan, J.-S. Han, G.-G. Xing, Role of the spinal cord NR2B-containing NMDA receptors in the development of neuropathic pain. *Exp. Neurol.* **215**, 298–307 (2009).
73. M. Liu, H. Yang, D. Fang, J.-J. Yang, J. Cai, Y. Wan, D.-H. Chui, J.-S. Han, G.-G. Xing, Upregulation of P2X3 receptors by neuronal calcium sensor protein VILIP-1 in dorsal root ganglions contributes to the bone cancer pain in rats. *Pain* **154**, 1551–1568 (2013).

74. G. Natura, G. S. von Banchet, H.-G. Schaible, Calcitonin gene-related peptide enhances TTX-resistant sodium currents in cultured dorsal root ganglion neurons from adult rats. *Pain* **116**, 194–204 (2005).
75. H.-H. Seo, C. Y. Lee, J. Lee, S. Lim, E. Choi, J.-C. Park, S. Lee, K.-C. Hwang, The role of nuclear factor of activated T cells during phorbol myristate acetate-induced cardiac differentiation of mesenchymal stem cells. *Stem Cell Res. Ther.* **7**, 90 (2016).
76. M. Ihara, N. Yamasaki, A. Hagiwara, A. Tanigaki, A. Kitano, R. Hikawa, H. Tomimoto, M. Noda, M. Takanashi, H. Mori, N. Hattori, T. Miyakawa, M. Kinoshita, Sept4, a component of presynaptic scaffold and Lewy bodies, is required for the suppression of alpha-synuclein neurotoxicity. *Neuron* **53**, 519–533 (2007).
77. K. Yang, C. Trepanier, B. Sidhu, Y.-F. Xie, H. Li, G. Lei, M. W. Salter, B. A. Orser, T. Nakazawa, T. Yamamoto, M. F. Jackson, J. F. Macdonald, Metaplasticity gated through differential regulation of GluN2A versus GluN2B receptors by Src family kinases. *EMBO J.* **31**, 805–816 (2012).
78. M. E. Hildebrand, J. Xu, A. Dedek, Y. Li, A. S. Sengar, S. Beggs, P. J. Lombroso, M. W. Salter, Potentiation of synaptic GluN2B NMDAR currents by Fyn kinase is gated through BDNF-mediated disinhibition in spinal pain processing. *Cell Rep.* **17**, 2753–2765 (2016).
79. E. C. Burgard, W. Niforatos, B. T. Van, K. J. Lynch, E. Touma, R. E. Metzger, E. A. Kowaluk, M. F. Jarvis, P2X receptor-mediated ionic currents in dorsal root ganglion neurons. *J. Neurophysiol.* **82**, 1590–1598 (1999).
80. Z.-J. Huang, X.-J. Song, Differing alterations of sodium currents in small dorsal root ganglion neurons after ganglion compression and peripheral nerve injury. *Mol. Pain* **4**, 20–24 (2008).
81. J. Tao, P. Liu, Z. Xiao, H. Zhao, B. R. Gerber, Y.-Q. Cao, Effects of familial hemiplegic migraine type 1 mutation T666M on voltage-gated calcium channel activities in trigeminal ganglion neurons. *J. Neurophysiol.* **107**, 1666–1680 (2012).
82. H. J. Meadows, C. G. Chapman, D. M. Duckworth, R. E. Kelsell, P. R. Murdock, S. Nasir, G. Rennie, A. D. Randall, The neuroprotective agent sipatrigine (BW619C89) potently inhibits the human tandem pore-domain K^+ channels TREK-1 and TRAAK. *Brain Res.* **892**, 94–101 (2001).
83. T. J. Coderre, N. Kumar, C. D. Lefebvre, J. S. C. Yu, A comparison of the glutamate release inhibition and anti-allodynic effects of gabapentin, lamotrigine, and riluzole in a model of neuropathic pain. *J. Neurochem.* **100**, 1289–1299 (2007).

Acknowledgments: We thank X. Gasull (University of Barcelona, Barcelona, Spain) for providing the rat TRESK plasmid. **Funding:** This work was supported by grants from the National Natural Science Foundation of China (81671085, 81371237, and 61527815) and the National Basic Research Program of China (2013CB531905). **Author contributions:** G.-G.X. conceived and designed the study and wrote the manuscript. Y.Y., S.L., Z.-R.J., and H.-B.J. conducted the experiments and analyzed the data. H.-Y.Z. and B.-H.L. assisted with immune-histochemical and biochemical experiments. Y.-J.L. and L.-Y.L. assisted with behavioral experiments. J.C. and Y.W. provided expertise and guidance. **Competing interests:** The authors declare that they have no competing interests. **Data and materials availability:** All data needed to evaluate the conclusions in the paper are present in the paper or the Supplementary Materials.

Submitted 29 July 2017
Resubmitted 27 May 2018
Accepted 20 September 2018
Published 16 October 2018
10.1126/scisignal.aao5150

Citation: Y. Yang, S. Li, Z.-R. Jin, H.-B. Jing, H.-Y. Zhao, B.-H. Liu, Y.-J. Liang, L.-Y. Liu, J. Cai, Y. Wan, G.-G. Xing, Decreased abundance of TRESK two-pore domain potassium channels in sensory neurons underlies the pain associated with bone metastasis. *Sci. Signal.* **11**, eaao5150 (2018).